

**STANDING POSTURE MODELING AND CONTROL
FOR A HUMANOID ROBOT**

SYEDA MARIAM AHMED

National University of Singapore

2013

**STANDING POSTURE MODELING AND CONTROL
FOR A HUMANOID ROBOT**

SYEDA MARIAM AHMED

*(B.Eng) National University of Sciences and Technology
(NUST), Pakistan*

**A THESIS SUBMITTED
FOR THE DEGREE OF MASTER OF ENGINEERING
DEPARTMENT OF MECHANICAL ENGINEERING
NATIONAL UNIVERSITY OF SINGAPORE**

2013

Declaration

I hereby declare that this thesis is my original work and it has been written by me in its entirety. I have duly acknowledged all the sources of information which have been used in the thesis.

This thesis has also not been submitted for any degree in any university previously.

A handwritten signature in cursive script, reading "Mariam", with a small flourish underneath.

Syeda Mariam Ahmed

August 19, 2013

Acknowledgements

First and foremost I am grateful to God, the Almighty, for blessing me with opportunities beyond my dreams and capabilities, for giving me the strength to achieve and succeed and for providing the best prospects to explore myself as a human being.

I would like to express my sincere gratitude and respect for my supervisor, Assoc. Prof. Chew Chee Meng, for trusting and giving me an opportunity to be part of one of the most exciting fields of robotics. During the two years of study, he has encouraged me through highs and lows, guided me in times of despair and helped me progress maturely.

I wish to thank my parents and my brother for their unswerving care and faith in my abilities, for making me capable enough to go this far in life and for inspiring me to achieve beyond my imagination.

I am grateful to my friends Umer, Amna, Bani, Juzar, Beenish and Nadia for their friendship and love during my stay at NUS, for being my family when I was away from home.

I would also like to thank my colleagues Wu Ning, Boon Hwa, Li Renjun and Shen Bingquan for their support and guidance during my research journey.

Author's Publication Related to Thesis

- Syeda Mariam Ahmed, Chee-Meng Chew and Bo Tian “Standing posture modeling and control for a humanoid robot”, *Proceedings of IEEE International Conference on Intelligent Robots and Systems* 2013.

Table of Contents

Acknowledgements	ii
Author's Publication Related to Thesis	iii
Table of Contents	iv
Summary	vi
List of Tables	vii
List of Figures	viii
Acronyms	x
List of Symbols	xi
1 Introduction	1
1.1 Motivation	1
1.2 Problem Statement	3
1.3 Research Focus	6
1.4 Approach	7
1.5 Thesis Outline	8
2 Literature Review	10
2.1 Background	10
2.2 Stability Criteria	10
2.3 Multidimensional Approach to Standing Stabilization	13
2.4 Conclusion	17
3 ASLAN Hardware Specifications	18
3.1 Background	18
3.2 Mechanics	19
3.2.1 <i>Dimensions</i>	20
3.2.2 <i>Actuators</i>	22
3.2.3 <i>Electronics</i>	22
3.3 Sensors	24
3.4 Software	25
3.5 Conclusion	25

4 Acrobot Modeling - Adaptive Parameter Estimation	26
4.1 The Acrobot Model	26
4.1.1 <i>Friction Approximation with Bipolar Sigmoid Function</i>	29
4.2 parameter Estimation	31
4.2.1 The Concept	31
4.2.2 <i>Estimation of Simplified Bipedal Model Parameters</i>	33
4.3 Implementation	37
4.4 Conclusion	42
5 Linear Control Design	43
5.1 Linearization of Non-Linear Model	44
5.2 Linear Quadratic Regulator-The Theory	47
5.3 Simulation Results in MATLAB	49
5.4 Conclusion	51
6 Partial Feedback Linearization	53
6.1 Partial Feedback Linearization- the Theory	53
6.2 Non-Collocated Partial Feedback Linearization (NCPFL)	54
6.3 Simulation Results in MATLAB	57
6.4 Conclusion	58
7 Full Body Control Architecture	59
7.1 Full Body Control	59
7.2 Implementation on WEBOTS	61
7.2.1 Simulation Setup	61
7.2.2 Implementation Details	63
7.3 Result Evaluation	64
7.4 Experimental Evaluation on NUSBIP-III ASLAN	70
7.4.1 Hardware Platform	70
7.4.2 Implementation Details	70
7.4.3 Results Evaluation	71
7.5 Performance Comparison with Passive Ankles	76
7.6 Conclusion	78
Bibliography	79

Summary

The work presented in this thesis focuses on modeling and designing a control strategy to balance a humanoid robot under a push, while standing. Stability has been comprehended as a vital aspect of mobility, extant in all mobile living things as part of an innate, subconscious ability. It is not an action that is preplanned or thought of during performance of any task by neither humans nor animals. On the contrary, this quality does not exist in humanoid robots and has to be integrated with all designed movements. Thus a control synergy of linear and non-linear control has been adopted, to stabilize a humanoid robot after it is pushed. The methodology has been tested in Webots simulator and subsequently on the robot ASLAN, resulting in successful stabilization of robots in both environments. The performance of the proposed controller has been compared with other control strategies, commonly employed in literature for the same objective. The advantage of employing the suggested method has been demonstrated with experiments. The intention is an attempt to mimic the human tiptoe behavior which leads to the introduction of an under-actuated degree of freedom around the toe. This maneuver can prove helpful under circumstances including difficult terrain or walking on stairs and can pave way for flexible and light weight feet, replacing the current heavy feet design for humanoid robot ASLAN.

KEYWORDS: Bipedal robot, acrobot model, linear quadratic regulator, partial feedback linearization

List of Tables

TABLE 1: DIMENSIONS OF THE ROBOT ASLAN	20
TABLE 2: MOTION AND MOTOR SPECIFICATIONS FOR LOWER BODY OF ASLAN	22
TABLE 3: FINAL PARAMETERS AND GAIN VALUES	35

List of Figures

Figure 1. Vision of DARPA grand challenge for humanoid robots to participate in a human society	2
Figure 2. Examples of position and force controlled humanoid robots	4
Figure 3. Difference in response to disturbance	5
Figure 4. Human attempting to balance by tiptoes, adding an un-actuated degree of freedom	8
Figure 5. Examples of point feet and flat foot robots respectively	11
Figure 6. Stable postures for humanoid robots	12
Figure 7. Contact positions and forces for force control approach to humanoid balancing	14
Figure 8. Linear inverted pendulum and double linear inverted pendulum model	15
Figure 9. <i>Ankle</i> , <i>hip</i> and <i>step</i> taking strategy based on simplified models	16
Figure 10. Models of humanoid robot ASLAN	18
Figure 11. ASLAN flat foot design	19
Figure 12. Workspace descriptions for <i>ankle</i> , <i>knee</i> and <i>hip</i> pitch joints	21
Figure 13. ASLAN electronics	23
Figure 14. Elmo whistle amplifier, used for controlling motors in ASLAN	23
Figure 15. Sensors on ASLAN	24
Figure 16. Humanoid robot modeled as acrobot	27
Figure 17. Response of Bipolar Sigmoid Function	29
Figure 18. Control architecture for adaptive algorithm	34
Figure 19. Results for tracking reference trajectory after tuning parameters through Adaptive Control	38
Figure 20. Results for parameter convergence through Adaptive Control	39-40
Figure 21. Simulation results for $x_0 = [0.02; 0.03; 0; 0]$	49
Figure 22. Simulation results $x_0 = [0.02; 0.03; 0; 0]$ with higher R value	50
Figure 23. Simulation results $x_0 = [0; 0.01; 0; 0]$ for upper body disturbance only	50
Figure 24. Simulation results $x_0 = [0.01; 0; 0; 0]$ for lower body disturbance only	51
Figure 25. Simulation results $x_0 = [-0.02; 0.03; 0; 0]$ using NCPFL and LQR	57
Figure 26. Simulation results $x_0 = [0.02; 0; 0; 0]$ using NCPFL	58

Figure 27. Full body control architecture	60
Figure 28. Humanoid simulation model in Webots	62
Figure 29. Simulation results for a forward push	64
Figure 30. Response of the humanoid robot to the applied push	65
Figure 31. Response of the humanoid robot to the applied backward push	66
Figure 32. Response of the humanoid robot to the applied push	67
Figure 33. Phase plot for multiple trajectories of CoM_{AVG}	68
Figure 34. Phase plots for state x for multiple trajectories	69
Figure 35. Response of humanoid robot ASLAN to a push from front and back	72
Figure 36. Response of humanoid robot ASLAN to a forward push	73
Figure 37. Response of humanoid robot ASLAN to a backward push	74
Figure 38. Response of the robot to multiple consecutive trajectories	75
Figure 39. Performance Comparison with Passive Ankle Joint	76
Figure 40. Performance Range for Controllers under Passive Ankle Joint	77

Acronyms

CoM	Center of Mass
CoP	Center of Pressure
CoG	Center of Gravity
DoF	Degree of Freedom
GRF	Ground Reaction Force
DC	Direct Current
GH	Gear Head
HD	Harmonic Drive
LIPM	Linear Inverted Pendulum Model
DLIPM	Double Linear Inverted Pendulum Model
PB	Pulley Belt
ZMP	Zero Moment Point
FZMP	Fictitious Zero Moment Point
FRI	Foot Rotation Indicator
DBFC	Dynamic Balance Force Control
VMC	Virtual Model Control
RTX	Real Time Extension
LQR	Linear Quadratic Regulator
PFL	Partial Feedback Linearization
NCPFL	Non-Collocated Partial Feedback Linearization
CPFL	Collocated Partial Feedback Linearization
LSE	Least Square Estimation
WLSE	Weighted Least Square Estimation

List of Symbols

$F(N)$	Force
$m_1(kg)$	Mass of link1 for Acrobot
$m_2(kg)$	Mass of link2 for Acrobot
$l_1(m)$	Length of link1 for Acrobot
$l_2(m)$	Length of link2 for Acrobot
$lc_1(m)$	CoM location for link1 for Acrobot
$lc_2(m)$	CoM location for link2 for Acrobot
$I_1(kg.m^2)$	Inertia of link1 for Acrobot
$I_2(kg.m^2)$	Inertia of link2 for Acrobot
$f_c(N)$	Coulomb friction
$f_v(N)$	Viscous friction
$q_1(rad)$	Link1 angular position
$q_2(rad)$	Link2 angular position
$\dot{q}_1(rads^{-1})$	Link1 angular velocity
$\dot{q}_2(rads^{-1})$	Link2 angular velocity
$\ddot{q}_1(rads^{-2})$	Link1 angular acceleration
$\ddot{q}_2(rads^{-2})$	Link2 angular acceleration
r	Sliding variable
e	Error in angular position
\dot{e}	Error in angular velocity
x	State for linearized model
u	Control effort for linearized model

CHAPTER 1

Introduction

1.1 Motivation

Since the past few decades, robotics has proved to be a domain catering ideas that transform structures to intelligent mechanisms for assisting humans, with minimal supervision. This requires design and control that has the capability to adapt to changes and interact with our environment. Thus, the innate ability of animals and humans to maneuver and acclimatize is harnessed and imitated, when it comes to the field of *robotics*.

Bipedal anthropomorphic structures are imagined to be the ultimate machines for the generations to come. Even though their role is still a highly debatable issue, it is nonetheless accepted as significant to human assistance in a wide domain of applications. Research in this particular domain has geared up to new heights in the past few years, resulting in robots like Petman by Boston dynamics [1].

Advancements in this particular field of robotics have already proven beneficial in the human world. Robotic manipulators with degrees of freedom equivalent to humanoid limbs are productive enough to be employed in industrial areas. Likewise, the replication of human legs is showing potential in the form of rehabilitative devices, prosthetics and exoskeletons.

Further enhancement in these domains requires an insight into mechanics and control of human locomotion. Recently, DARPA introduced a humanoid robotics challenge which requires humanoid robots to perform search and rescue missions, operate machinery and navigate their way around a dynamically changing environment, as shown in Figure 1, where robot HUBO demonstrates tasks that need to be performed in order to participate in a human society. This challenge provides a glimpse of what the future might hold for research in humanoid robotics.



Figure 1. Team DRC-HUBO [2] prepares for DARPA grand challenge

In an attempt to emulate human behavior for optimal performance, researchers have discovered that the concept of *stability* is a prerequisite for successful implementation of any task. Despite being an innate quality in all living things, the idea of stability for robots presents itself as a complex domain of its own. It spans

from the appropriate mechanical structure, to swiftness of control and powerful yet compliant actuation in order to achieve basic standards of stability.

There have been various attempts to quantify and qualify the phenomenon through stringent criteria which might prove to be successful for a particular task, but hold little meaning when it comes to others. Nonetheless, there is still a struggle to coin a generic definition which could cater stability and prove useful for robots with varying physical features and work descriptions.

The *motivation* behind this work is an attempt to implement stability for bipedal humanoid robots while standing, exploring the strength of upper body agility for stabilization. Since the demand for these robots to participate in a human society has drastically increased over the past decade, it is important to comprehend stability in humans and ultimately implement the notion as an integral part of each robotic behavior.

1.2 Problem Statement

Bipedal robots are accompanied with high dimensional non-linear dynamics which adds to the complexity of the control of such mechanisms. They have intervals of continuous and discrete dynamics during single support phase and at foot impact, respectively, which adds to this complexity. The narrow base of support during walking and the effects of collision between the foot and the ground also make the biped essentially unstable.

The nature of the disturbance and instability presented by the issues mentioned above is also dependent on the method of actuation of robots. One method includes *position controlled robots*, shown in Figure 2a, which are equipped with electric

motors and harmonic drive systems. The high gear ratio makes the joints highly stiff which can reject small disturbances effectively, but at the same time, cannot cater larger disturbances. Due to these characteristics, these robots can efficiently track a pre-defined trajectory, but are incapable of adapting to the environment changes.

On the other hand, *force controlled robots*, shown in Figure 2b, employ direct drive actuation, commonly through hydraulic or series elastic actuators. These provide the advantages of compliance and interaction with the environment as opposed to the position controlled robots. Therefore, they are based on impedance control where the degree of compliance for various scenarios may be tuned according to requirement; otherwise they may become highly susceptible to instability due to small disturbances produced by their own gait. This type of actuation accentuates the complexity of control but reflects greater similarities to a human as compared to other robots.



a) ASIMO



b) Petman

Figure 2. Examples of position [3] and force controlled [1] humanoid robots

The concept of *push recovery* is derived from the ability of a robot to be able to balance itself under influence from external forces. Even though the methods of actuation described above, result in a different response to these forces as shown in Figure 3, maintaining balance is a problem nonetheless. The issue addressed in this thesis aims to attain balance and maintain posture while standing for a *position controlled* humanoid robot. The challenge involves catering the stiffness and high rigidity of individual joints, along with achieving rapid control response to induced disturbance. Furthermore, the idea of stability with passive ankle joint is explored to comprehend the possibility of eliminating the heavy weight feet of our humanoid robot ASLAN which hinder swift mobility of the bipedal robot.

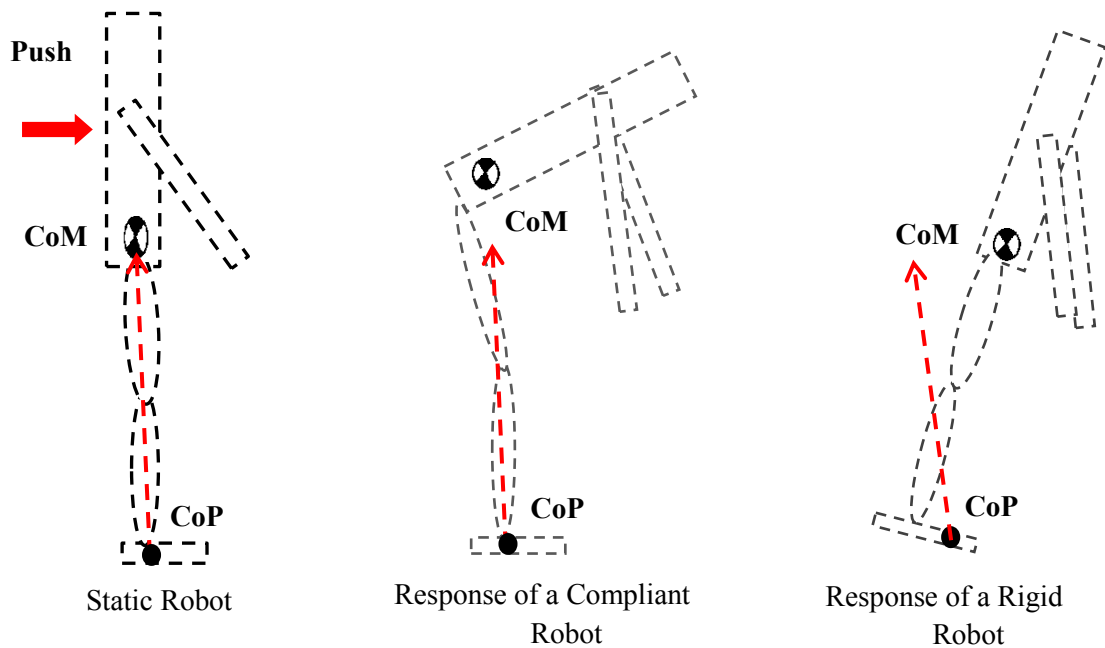


Figure 3. Difference in response to disturbance

1.3 Research Focus

The main *focus* of this research is to implement stability in a *position controlled* humanoid robot, in a manner that mimics a human's response to applied disturbance. Conflict for such robots exists in the rigidity and non-back drivable nature of their joints. Such characteristics eliminate the advantage of a multiple degree of freedom robot, while inculcating a structural response to disturbance.

Another aspect for consideration of position controlled robots is the necessity of harmonic drive or pulley systems connected to DC motors, to increase the magnitude of deliverable torque. These components induce *non-linear friction* in joints, which necessitates model identification at each joint, which is a highly difficult task in itself. This friction is dependent on the gear ratio for individual joints. The friction along with added weight of the actuation mechanism, especially in the lower body, results in slow maneuverability for the robot.

The problems identified are the key issues due to which a position controlled robot generally stabilizes itself by taking a step in the direction of the push, as implemented on ASIMO [3]. However, this is not a solution which is applicable under circumstances where maintaining position is necessary.

Keeping these issues in mind, the aim of this work is to instill autonomous stability for position controlled humanoid robots, attempting to add compliance in the overall upper and lower body of the robot so as to mimic human flexibility. This research will also attempt to cater friction components at the actuated joints, in order to improve dynamic control of the system.

1.4 Approach

The approach adopted in this thesis is an extension to using simplified models that represent and predict the dynamic behavior of the robot. This approach has been employed by various researchers in the past; varying in the specific model and in turn the dynamics they chose to depict the humanoids response. The model employed in this work is an acrobot model, similar to the double inverted pendulum (DIPM), but differing in terms of actuation [4].

Primary objective remains to instill the capability of responding to a disturbance in a manner that adds compliance to the system. However, the methodology chosen maximizes dependency on the hip joint rather than ankle joint. The reason behind employing this behavior is to derive a control strategy which relies on upper body actuation and assumes passivity at the ankles. This approach is adopted in order to explore the effectiveness of a hip joint to sustain balance, investigating whether it is possible to stabilize the robotic system without the extant ankle joint. Eliminating the compulsion of the ankle joint can lead to weight reduction by removing it from our humanoid robot NUSBIP III ASLAN. This in turn can facilitate swifter movement of the swing leg due to lighter inertia, especially as viewed from the hip joint.

The possibility of this maneuver is derived from the human act of ‘balancing on tiptoe’, which adds an un-actuated degree of freedom at the toe fingers, as shown in Figure 4. Humans in particular employ this behavior while walking on stones or rugged terrain where a limited contact area is advantageous.

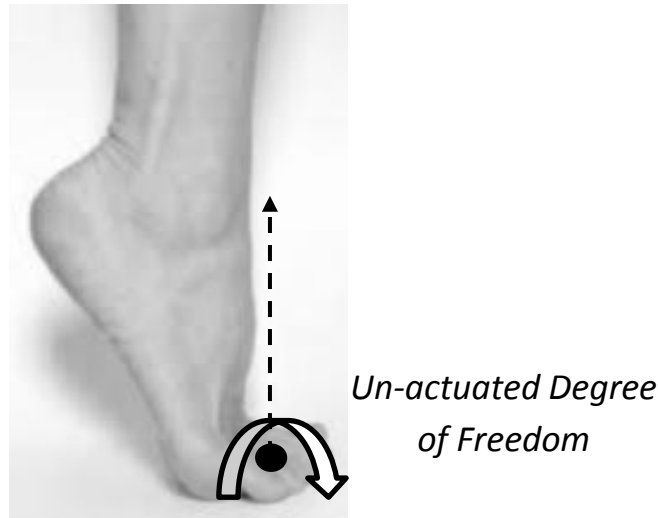


Figure 4. Human attempting to balance by tiptoes, adding an un-actuated degree of freedom [5]

However while doing so, humans employ three actuated joints (at the hip, knee and ankle in the sagittal plane) with a single passive joint (at the tip of the toe), along with upper body actuation, to sustain balance.

Similarly, this thesis explores whether a single joint at the hip has the capacity to provide stability in presence of a passive ankle joint. The concept presented can be further extended to employ knee joints for additive support. For this purpose an acrobot model is employed instead of a double inverted pendulum model, which captures the characteristics of a passive ankle joint. Thus, balancing with a higher level of reliance on upper body maneuvers, in presence of an un-actuated ankle joint, is the specific aim of this research.

1.5 Thesis Outline

Having presented the aims and objectives of the thesis, it is important to be aware of the work that has been done by previous researchers, in this particular domain. Chapter 2 presents an overview of the related work regarding standing stabilization,

followed by chapter 3 which presents an introduction to the robot NUSBIP-III ASLAN and its hardware specifications. Chapter 4 describes the procedure involved in dynamic modeling of the behavior of the humanoid robot, and the technique employed to carry out parameter estimation. Chapter 5 describes linear feedback control, an attempt to solve the problem of stabilization using the simplest methodology available in literature. However, due to unsatisfactory results, chapter 6 details the theory behind partial feedback linearization for lower body stabilization of the robot. Chapter 7 presents a complete control architecture tested in Webots simulator and implemented on the robot ASLAN.

CHAPTER 2

Literature Review

2.1 Background

When a human is pushed, the impulsive reaction is a synergy of control actions adopted by our upper and lower body. Multiple degrees of freedom in a human provide the ability to sustain balance despite constraints on individual joints. For humanoid robots, push recovery has been investigated diversely in terms of varying control objectives. This chapter provides a comprehensive understanding towards the concept of bipedal stabilization during standing and reflects upon the methodologies employed in this domain. Variation in stability criteria for humanoid robots is highlighted, followed by an overview of approaches and push recovery models.

2.2 Stability Criteria

The most common concept that is used to define stability in a legged robot is the zero moment point (ZMP). The idea of ZMP was introduced by M. Vukobratovic for the analysis of stability in bipedal robots. ZMP may be defined as the point on the ground where the sum of all moments due to forces between the foot and the ground,



Mabel – Point Foot Robot



HRP– Flat Foot Robot

Figure 5. Examples of point feet [7] and flat foot [8] robots respectively

becomes zero [6]. In consequence, stability for any desired trajectory arises from the notion of maintaining the ZMP within the support polygon of the robot. The support polygon of a robot is represented by the area enclosed by a foot or feet on the ground. Figure 5 shows the variation in feet for humanoid robots. For a point foot robot, the support polygon is a straight line between the point feet of the robot, while for a flat foot robot, the entire area enclosed by the robot's feet is its support polygon. For these robots, if the ZMP lies at the edge of the support polygon, the trajectory may not be feasible. This concept is similar to the Center of Pressure (CoP), which is also a point where the resultant reaction forces between the ground and foot act in a plane parallel to the ground. However, this point is directly measured from the ground reaction forces through force sensors at the edges of the foot, whereas ZMP may also be computed analytically based on the state of the robot.

Foot Rotation Indicator (FRI) is a slightly general form of the idea that revolves around ZMP and CoP [9]. It is the point on the ground where the net ground reaction force should act to maintain a stationary position for the foot. Thus, FRI is not limited to the edge of the support polygon in case of rotation, unlike ZMP and CoP, but rather indicates a new desired position for CoP which may be used for control purposes.

Another domain of robots includes passive dynamic walkers with curved feet or point foot bipedal robots [10, 11]. The concepts of ZMP and CoP have little meaning for these robots due to the mechanical design of their feet. For a point foot robot, the ZMP or CoP location is restricted to a single point and theoretically indicates a zero stability margin. Contrary to theory, bipedal robots like Mabel from Michigan University have proved walking stability for point foot robots. Thus a new concept of Poincare maps is introduced for these robots, which defines cyclic stability during walking [12].



Figure 6. Stable postures for humanoid robots

Capture point theory [13-15] and velocity based stability margins [16] are other popular stability criteria referred by researchers, where the former defines stepping locations for a biped in case of a larger degree of disturbance, while the latter defines stability in terms of velocities of states.

The idea of standing stability can be generalized to satisfying the criterion of collinearity of CoP/ZMP and center of gravity (CoG). As long as the two points are collinear in every plane, the robot can stabilize at any desired posture. Figure 6 shows Bioloid [17] and Darwin [18] robots which are small sized robots, developed for robotic soccer competitions and other applications. The diversity in standing postures including balancing on one leg, are achieved based on the same criterion.

Even though the condition for balancing while standing, on one or two legs, is understood, sustaining it under disturbance is difficult. The next section elaborates on the extant strategies adopted and implemented on humanoid robots, to achieve balance in presence of disturbance in their environment.

2.3 Multidimensional Approach to Standing Stabilization

Despite having definitive stability criteria, it is still difficult to generalize one particular method and apply it to all existing humanoid robots. The reason is based on diversity in mechanical and actuation designs of the system, which play an important role in determining stability margins for maintaining balance. This section gives an overview of the different approaches employed by researchers for stabilizing humanoid robots under disturbance.

Force controlled robots generally have a capacity to provide higher torque as compared to DC motors. These systems also have an innate capacity to be compliant

as opposed to rigid structures of position controlled robots. Due to this ability, such robots can easily distribute external forces or disturbance across their structure. DLR-Biped and Sarcos robots are examples of such force controlled robots that have successfully demonstrated standing balancing and posture regulation.

For these robots, balance has been achieved through contact force control, as shown in Figure 7. This approach employs passivity based controllers where optimal contact force distribution

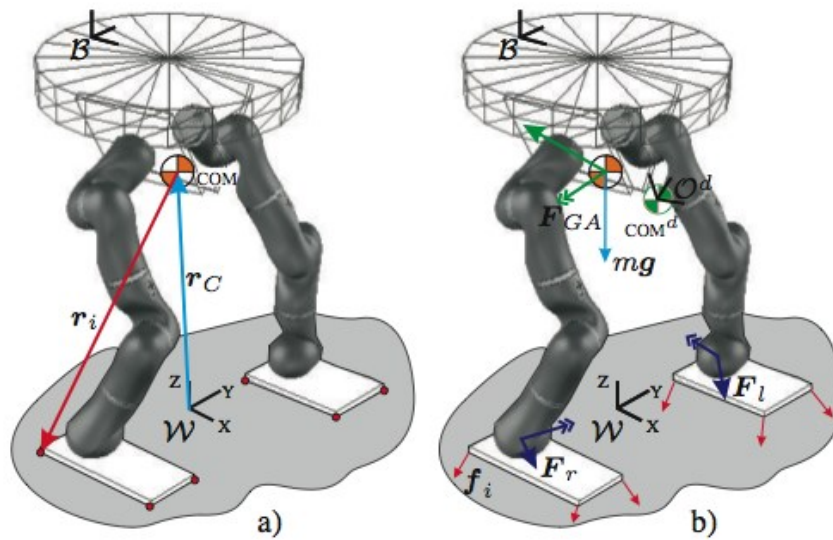


Figure 7. Contact positions and forces for force control approach to humanoid balancing [19]

leads to desired ground applied forces (GAF) converted to joint torques [20-23]. Dynamic balance force control (DBFC) is another method which uses virtual model control (VMC) to perform posture regulation for Sarcos Primus [24].

A similar method deals with defining desired rate of change of angular and linear momentum, based on computation of individual foot ground reaction forces (GRF) and CoP [25]. This approach is motivated by the idea that humans regulate their angular momentum about the CoM to perform various motions. The amount of

angular momentum that can be provided to sustain balance is limited by joint angle workspace and actuator limitations. Thus dynamic stabilization through optimization under constraints imposed by ground contact and joint limits, has also been attempted [26,27].

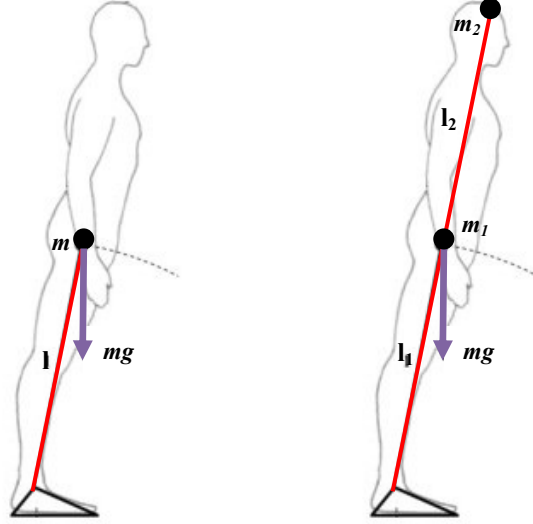


Figure 8. Linear inverted pendulum and double linear inverted pendulum model [28]

A slightly different approach which serves as the foundation for this research is to reduce the humanoid to simple models, shown in Figure 8, and analyze their behavior in presence of disturbance. Kajita, et.al. proposed modeling of a biped as a *Linear Inverted Pendulum Model* (LIPM) [29]. The system is assumed to have lumped mass at the end of a link which represents the effective center of mass (COM) location for the robot. The single link represents the lower body, assuming combined movement of the two legs at all times.

A similar model is *Double Inverted Pendulum* which was proposed by Hemami et.al. [30]. This model describes the upper and lower bodies of the humanoid as individual links, with a lumped mass for each link located at the CoM position. These linearized models constrained in one-dimensional plane are controlled to yield desired

ankle and hip trajectories which ensure CoM regulation above CoP, fulfilling criterion for standing stability [31].

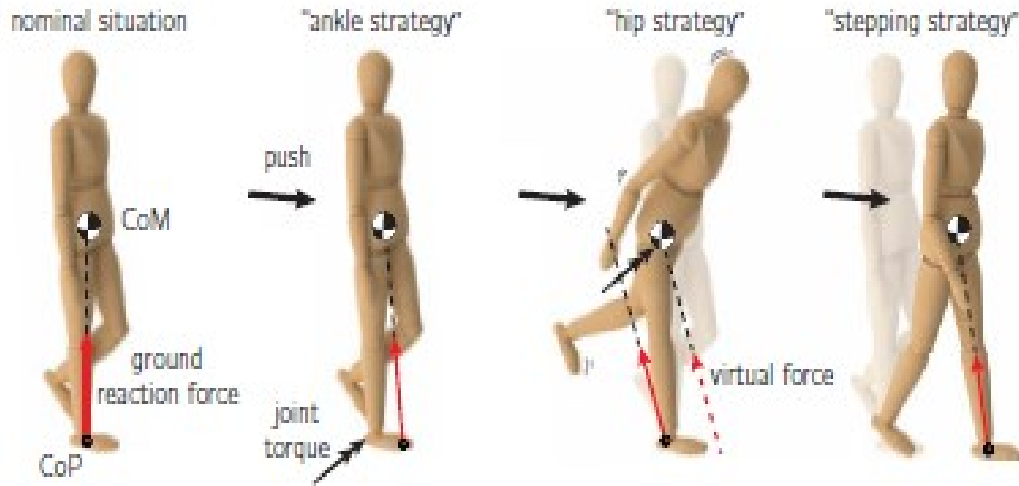


Figure 9. *Ankle, hip and step* taking strategy based on simplified models [32]

These models have also been used by biomechanists to explain balancing through *ankle* and *hip* strategies for humans [33], illustrated in Figure 9. Modern *ankle* strategy for humanoid robots essentially abides by the ZMP theory and suggests employing ankle torque to regulate CoP within the convex hull formed by the support polygon. *Hip* strategy on the other hand, is used when ankle torque cannot alone sustain balance, and a restoring torque is applied at the hip in an attempt to restore center of mass (CoM). Step strategy is proposed for a disturbance so large that a fall becomes inevitable by remaining in the same position.

Simple model strategy implies dependence on ankle torque as a primary source of maintaining balance, as reflected by the proposed *ankle* strategy in literature. On the contrary, the approach adopted in this paper aims to maximize dependence on hip joint.. Thus, this thesis models the humanoid robot as an acrobot, to enable design of a

control strategy which can harness the strength of the hip joint, in terms of high torque capacity as compared to other joints in the lower body.

2.4 Summary

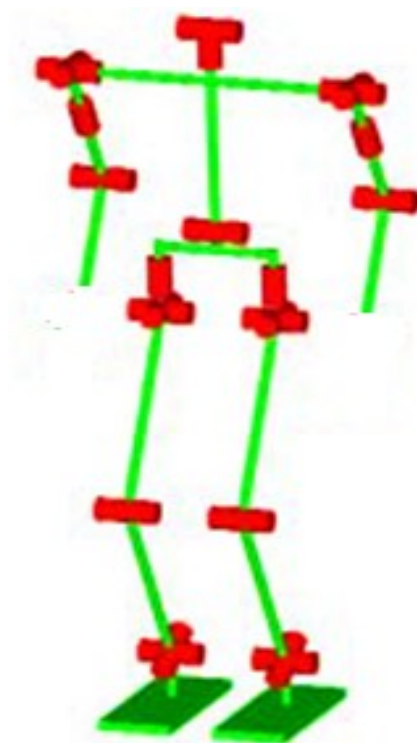
This chapter provides a comprehensive overview of the extant strategies generally employed for stabilization for humanoid robots. Simplified model approach, where basic models including linear inverted pendulum and double linear inverted pendulum have been particularly highlighted, since the same idea has been extended in this work.

CHAPTER 3

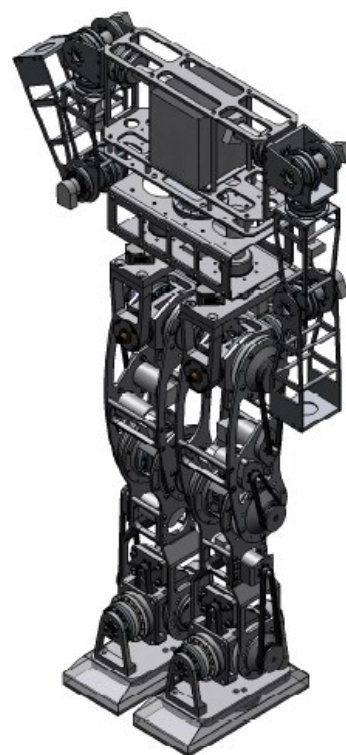
ASLAN Hardware Specifications

3.1 Background

The humanoid robot NUSBIP-III ASLAN is a successor of multiple legged robot platforms, namely the ROPE series, designed by the Legged Locomotion Group (LLG) at National University of Singapore. The 3D model of this robot and its CAD drawing is shown in Figure 10. Previous robots were '*kid-size*' robots, limited in



a) 3D Model of ASLAN



b) CAD drawing of ASLAN

Figure 10. Models of humanoid robot ASLAN

height and weight. However, NUSBIP-III is a human-sized robot which was developed around 2008, primarily to study bipedal walking [34,35]. Till now, the robot has demonstrated successful walking on even terrain, slope and stairs [36]. The robot also participated in ROBOCUP humanoid adult size category in 2010 and won first prize.

3.2 Mechanics

ASLAN is a complete humanoid robot with a head, trunk, arms and legs. Lower limbs are equipped with six degrees of freedom (DOF) each. For each leg, three joints exist at the hip, one at knee and two at the ankle. While for the arms, three DOF exist at the shoulder and one at the elbow. Head of the robot is equipped with a single camera based vision system, where the neck allows pitch and yaw movement. The trunk is designed to carry the bulky electronics, sensors and batteries. The waist has a single DOF enabling swinging motion of the upper body through yaw movement.

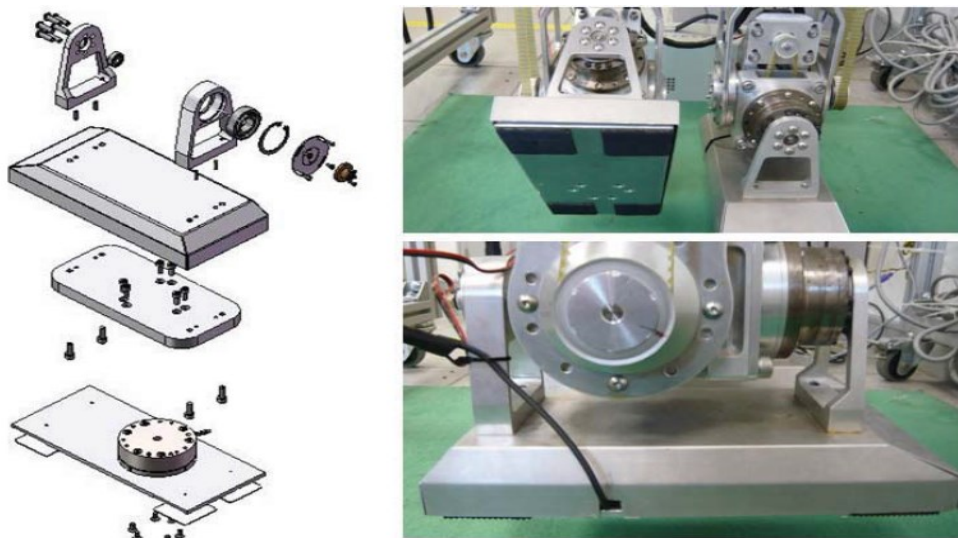


Figure 11. ASLAN flat foot design [37]

The robot ASLAN is a flat footed robot, illustrated in Figure 11. The foot design consists of an aluminum plate consistent of force/torque sensor to detect force value at impact. The foot is also equipped with rubber padding for impact absorption which is easily replaceable, thus facilitates maintenance.

3.2.1 Dimensions

The research regarding balancing is restricted to sagittal plane, thus parameters for the humanoid are extracted for this particular plane only. Detailed parameter estimation is carried out using adaptive control, which will be explained in chapter 4, but nonetheless, a rough estimate of dimensions is required in order to achieve convergence within a specified range. Thus the basic inertial dimensions are calculated from the CAD drawings of the robot, where the parameters are tabulated as follows. The values shown below do not include weight added by the motors and electronics.

Table 1. Dimensions of the robot ASLAN

Body	Length / mm	Mass /Kg
Foot	121	3.3 x 2
Shank	280	4.5 x 2
Thigh	280	2.8 x 2
Upper Body	479	13.2

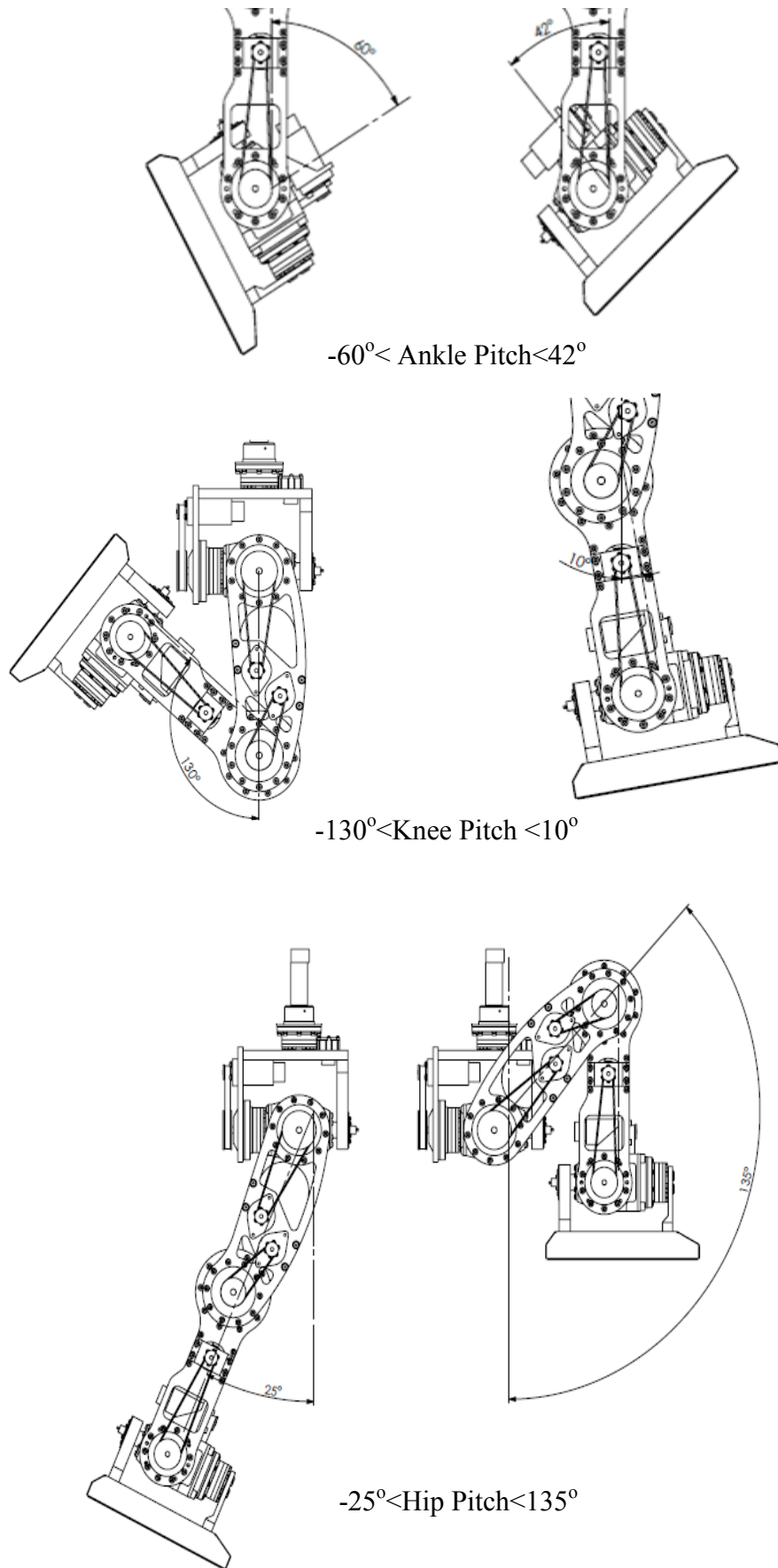


Figure 12. Workspace descriptions for *ankle*, *knee* and *hip* pitch joints

3.2.2 Actuators

All joints are connected to the motors through either harmonic drive or a combination with belt driven system. The aim is to provide higher torque and accuracy with zero backlash. However, this combination adds rigidity and high friction components to the system, which will be catered, to some extent, through parameter estimation.

Table 2. Motion and motor specifications for lower body of ASLAN

Joint	Range of motion/Deg	Motor Power/watt	Gear Ratio
Hip Pitch	-45 to 135	200 Brushless motor	160:1
Knee Pitch	-130 to 10	200 Brushless motor	160:1
Ankle Pitch	-45 to 20	150 Brush motor	120:1

The allowed workspace configurations have been shown in Figure 12 for each joint. The maximum current rating for the motors has been given in Table 2. A 200 Watt Maxon motor has been used at the hip pitch joint which can provide up to 9 amperes of continuous current. Knee and ankle pitch motors have a comparatively lower power rating of 150 Watt, which can regulate 6 amperes of continuous current.

3.3 Electronics

ASLAN consists of a single onboard computer, PC/104, which communicates with the motors through ELMO Whistle amplifiers, via a CAN BUS board, shown in Figure 13 and 14 respectively. ELMO is locally tuned to execute accurate position

control. However, the work described in this thesis operates the motors in current mode, which is implemented without any auto-tuning within ELMO.

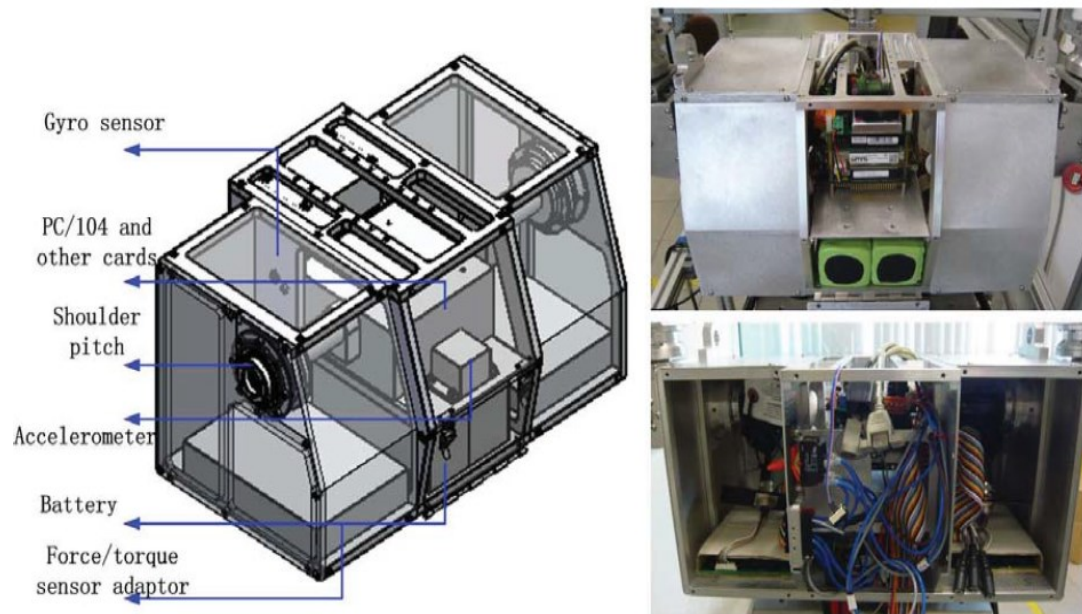


Figure 13. ASLAN electronics [37]

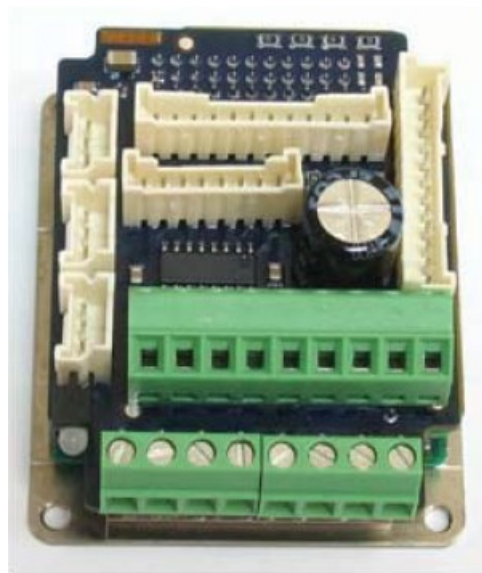


Figure 14. Elmo whistle amplifier, used for controlling motors in ASLAN [37]

3.4 Sensors

The robot has various sensors, illustrated in Figure 15, to measure orientation of the system and individual links. MAE3 Absolute encoders are mounted on the robot which can provide absolute position of a joint, essential for keeping track of posture and re-initialization. Encoders mounted at the shaft of the motor are used for more accurate position tracking purposes. With the exception of yaw joint at the hip, all other DOF in the lower body are equipped with this sensor. Due to mounting challenges, the hip yaw joint has a wire sensor encoder.

An inertial measurement unit is developed by employing accelerometer and gyroscopes at the trunk of the robot. The sensors are connected to the PC through a DAQ board which converts analog signals from the sensors to digital form.



MAE3 Encoder



Wire Sensor Encoder



Accelerometer



Force\Torque Sensor

Figure 15. Sensors on ASLAN [37]

Subsequent kalman filtering on extracted data results in an accurate estimate of the orientation of the robot.

3.5 Software

The robot is controlled through the real time extension (RTX) software in Windows. RTX is a package which enables real time computation in Windows, with a sampling time of 10ms. However, the version of RTX used cannot communicate with ELMO driver. Thus a shared memory is created which serves to communicate between ELMO and main program running under RTX. All coding has been carried out in C++. Control strategies are implemented in the main program, updating relevant information in the shared memory, at every sampling time, which in turn updates the execution at the ELMO program. This communication loop ensures real time implementation of controllers on the robot.

3.6 Summary

The humanoid robot ASLAN, introduced in this chapter, is used for evaluation and testing of the designed control strategy for push recovery. The robot will be controlled in a current mode, assuming a linear relationship between torque and current. The workspace and actuation limitations of the system play an important role in identification of optimal methodology to sustain balance.

Chapter 4

Acrobot Modeling - Adaptive Parameter Estimation

The approach adopted in this work aims to maximize dependence on hip joint and subsequent upper body movements to sustain balance. The idea stems from the tiptoe maneuver in a human, commonly employed in uneven terrain situations. Mechanical design for humanoid foot has not yet advanced to a level where a compliant foot may be designed, which has the capacity to balance on the tip of the toes like humans. Nonetheless, the approach provides a means of deriving a control strategy that has lower torque requirements from the ankle joint, and can pave way for such a possibility to inculcate robustness and greater efficiency in humanoid robots. Thus, the following section describes modeling of the bipedal robot, ASLAN, as an *acrobot*, which is a double inverted pendulum with a passive ankle joint.

4.1 The Acrobot Model

The acrobot is a commonly used two bar linkage system, which is stabilized vertically upwards. Despite having two degree of freedoms, one of the joints at the base is un-actuated while the other is actuated. This system is extensively studied to solve the stabilization problem using various techniques.

The humanoid robot in its sagittal plane is modeled as this two link acrobot, where the lower and upper body forms link one and two respectively. Using the lagrangian

system of equations to express the model of the bipedal robot as an acrobot, as shown in Figure 16, yields the following equations [38],

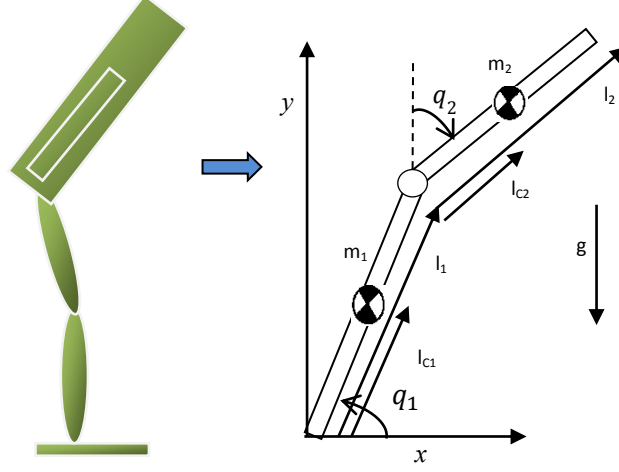


Figure 16. Humanoid robot modeled as acrobot

$$d_{11}\ddot{q}_1 + d_{12}\ddot{q}_2 + C_1 + G_1 + F_1 = 0 \quad (1)$$

$$d_{21}\ddot{q}_1 + d_{22}\ddot{q}_2 + C_2 + G_2 + F_2 = \tau_{Hip} \quad (2)$$

where,

$$d_{11} = m_1 l_{c1}^2 + m_2 (l_1^2 + l_{c2}^2 + 2l_1 l_{c2} \cos(q_2)) + I_1 + I_2$$

$$d_{22} = m_2 l_{c2}^2 + I_2$$

$$d_{12} = m_2 (l_{c2}^2 + l_1 l_{c2} \cos(q_2)) + I_2$$

$$d_{21} = d_{12}$$

$$C_1 = -m_2 l_1 l_{c2} \sin(q_2) \dot{q}_2^2 - 2m_2 l_1 l_{c2} \sin(q_2) \dot{q}_2 \dot{q}_1$$

$$C_2 = m_2 l_1 l_{c2} \sin(q_2) \dot{q}_1^2$$

$$G_1 = (m_1 l_{c1} + m_2 l_1) g \cos(q_1) + m_2 l_{c2} g \cos(q_1 + q_2)$$

$$G_2 = m_2 l_{c2} g \cos(q_1 + q_2)$$

where q is the 2×1 vector of joint displacements, τ is the 2×1 vector of applied torques, $D(q)$ is the 2×2 positive definite inertia matrix. C is the 2×1 vector of centripetal and coriolis torques, $G(q)$ is the 2×1 vector of gravitational torques and F is the 2×1 vector of frictional torques induced by the gears and bearings in the robot. The friction model used is of the form,

$$F(\dot{q}) = f_c \text{sgn}(\dot{q}) + f_v \dot{q} \quad (3)$$

where f_c and f_v represent coulomb and viscous friction parameters [39], respectively. The primary reason for using this friction model is that can be estimated using simple trajectory and velocity profiles. This is particularly advantageous since the motors and gears are assembled with the humanoid links and individual identification through complicated procedures is not possible. The $\text{sgn}(\dot{q})$ function is defined as,

$$\text{sgn}(\dot{q}) = \begin{cases} -1, & \dot{q} < 0 \\ 0, & \dot{q} = 0 \\ 1, & \dot{q} \geq 0 \end{cases} \quad (4)$$

Based on these equations, the upper and lower body dynamics of the humanoid robot are coupled. However, friction components extant as part of the lagrangian equation of upper link, reflect friction at the hip joint only, while those in the lower links represent friction at the ankle joints. Since all other degrees of freedom in the sagittal plane, including knee joints and upper body limb joints, remain rigid, their friction components are ignored by the model. This model also assumes that both legs move together at all times, therefore are modeled as a single link.

4.1.1 Friction Approximation with Bipolar Sigmoid Function

The friction model employed for parameter estimation was defined as,

$$F = f_c \operatorname{sgn}(\dot{q}) + f_v \dot{q}$$

If this model is linearized, the coulomb friction component will reduce to zero. Thus the $\operatorname{sgn}(\dot{q})$ function is replaced by a bipolar sigmoid function which behaves almost exactly like the $\operatorname{sgn}(\dot{q})$ function. This bipolar sigmoid function is defined by the following equation,

$$\operatorname{bipolar}(\dot{q}) = f(\dot{q}) = \frac{1 - e^{-\dot{q}\alpha}}{1 + e^{-\dot{q}\alpha}}, \quad \alpha = 10 \quad (5)$$

Equivalence of these two models for a range of $-3\pi < \dot{q} < 3\pi$ has been verified in Matlab.

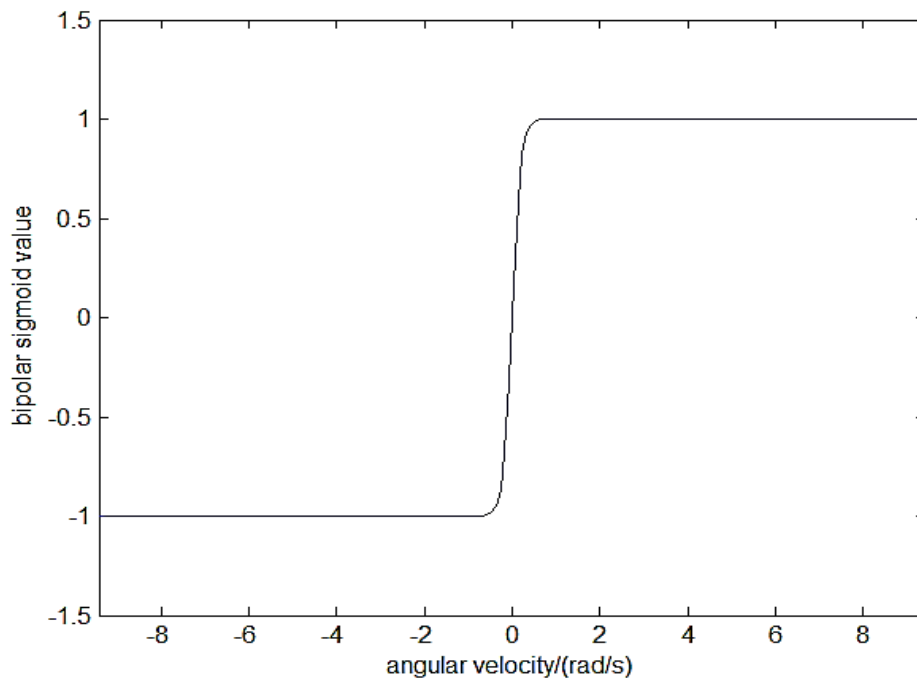


Figure 17. Response of bipolar sigmoid function

The use of bipolar sigmoid term provides a continuous function, simplifying differentiation for linearization of non-linear model for control design, unlike $sgn(\dot{q})$ function. The graph in Figure 17 shows the response of the bipolar sigmoid function, in the range assigned, proving that this function behaves like the one described previously. Derivation of this function with respect to velocity of the respective joint yields the following function,

$$\frac{\partial bipolar(\dot{q})}{\partial \dot{q}} = \frac{\alpha}{e^{\dot{q}\alpha}(\frac{1}{e^{\dot{q}\alpha}} + 1)} - \frac{\alpha(\frac{1}{e^{\dot{q}\alpha}} - 1)}{e^{\dot{q}\alpha}\sqrt{(\frac{1}{e^{\dot{q}\alpha}} + 1)}}, \quad \alpha = 10 \quad (6)$$

Which can be further simplified to take a form as follows,

$$\frac{\partial bipolar(\dot{q})}{\partial \dot{q}} = \frac{\alpha}{2 \cosh(\frac{\alpha * \dot{q}}{2})} \quad (7)$$

It can be seen from the equation above, that this function does not go to zero as the velocity of the system goes to zero at the equilibrium point. Thus the following model is used to define the friction model,

$$F = f_c \frac{1 - e^{-\dot{q}\alpha}}{1 + e^{-\dot{q}\alpha}} + f_v \dot{q} \quad \alpha = 10 \quad (8)$$

4.2 Parameter Estimation

4.2.1 The Concept

Parameter estimation is an essential prerequisite to control of a bipedal robot which involves a comprehensive knowledge of the kinematic and dynamic features of individual links and actuators. Ideally, these should be identified before the assembly of these parts in order to maintain accuracy [40-41]. In many cases, inertial parameters including mass of links, center of mass locations, moment of inertia etc. are calculated from CAD drawings of the robot. Nonetheless, these drawings do not cater the added electronics and actuation system which contribute to added friction, inertia and total mass of the robot, essentially changing all the parameters previously determined. Thus the concept of '*parameter estimation*' takes its place, analyzing input-output behavior of the robot in order to estimate the relation between the two.

Least square estimation is one of the most common and thoroughly researched strategies in literature which aims to minimize the difference between the actual output and estimated output from the model, over a series of predefined trajectories [39,42]. The standard model of the system is defined in terms of Lagrangian equations, converted to a linear parametric form, defining the input output relation as,

$$\tau = \varphi(q, \dot{q}, \ddot{q})\theta \quad (9)$$

Generally, torque is the input while joint position trajectory is the output. $\varphi(q, \dot{q}, \ddot{q})$ is the regressor matrix which is responsible for defining variables that govern the relation between input and output.

There are two major aspects that define the feasibility and success of this concept in practice. First is the identification of suitable trajectories which have the capacity to excite the dynamics of the entire robot [43]. Researchers have aimed to solve this issue by employing fourier series and calculating their respective coefficients through optimization strategies, under the constraints imposed by workspace boundaries of the links in terms of position, velocity and acceleration [44]. Those who found this tedious have attempted adding higher order polynomials to fourier series, where the coefficients are found during parameter estimation [45]. Nonetheless, whether these identified trajectories are aptly exciting for the given system is only determined after a series of experimental results. If the inertial parameters turn out to be negative in number, it is suggested that the trajectory was unable to excite the system, thus moving the entire procedure back to square one.

Second hurdle is obtaining appropriate and noise free sensor readings. In some cases, force-torque measurements are obtained by torque sensors installed at every joint of the robot, which makes estimation relatively simpler. Otherwise, torque to a joint needs to be estimated through current, assuming a linear relationship as follows,

$$i = \frac{\tau}{K_T N} \quad (10)$$

where N is the gear ratio and K_T is the torque constant, obtained from the motor datasheet. Since the humanoid robot NUSBIP-III ASLAN is not equipped with torque sensors, this particular relationship is used to desired current. The Elmo motion controller which commands current to the motors is used to keep track of current readings at every instant. It is to be noted that this linear relationship holds true as long as the system remains in a close vicinity to the equilibrium position of the

system, described in chapter 5 as the stabilized state for the robot. Experimentations detailed in the proceeding sections verify that slight variations due to this assumption does not affect the overall performance of the system to a great extent.

Literature reports that these torque constants vary up to 25% from their reported values during loading, thus adding another uncertainty to the system [43]. Also, the quantization error in position readings from the encoders, affects the velocity and acceleration, due to calculation by numerical differentiation. The resulting inaccuracy has a significant effect on the estimation procedure since the methodology originally relies heavily on accuracy of input and output readings.

Weighted least squares method is a proposed modification to the least squares where the covariance of noise is assumed to be known and is added to the estimation procedure, to cater the noise in sensor readings [46]. Even though this method performs much better than its predecessor, the accuracy of estimated parameters is still questionable.

Alternative approaches include Newton-Euler method and energy based model where the former requires force-torque sensor measurements while the latter requires only position and velocity variables, without the need of noise ridden acceleration readings [47-50]. However, the energy based model relies on the integration of torques and joint velocities to determine energy which adds an unknown bias to the readings.

4.2.2 Estimation of Simplified Bipedal Model Parameters

In light of the previous methods presented for parameter estimation, it is extremely difficult to implement these on an assembled bipedal robot. Underactuation of the

robot makes it effectively unstable for a random trajectory. Appropriate trajectories which have the excitation capacity and cater all links of the bipedal robot are extremely difficult to design and depend on manual tuning which becomes a task on its own.

For our bipedal robot ASLAN, inertial properties of individual links are obtained from CAD. However, control objectives require the bipedal robot to be modeled as a double inverted pendulum with a passive ankle, essentially as an ‘*acrobot*’. This aggregates the two legs as one link while leaving the feet out, since the ankles are passive. Similarly, the torso, trunk, head and arms are combined to form the second, upper link. Thus adaptive algorithm is used for parameter estimation of the simplified model.

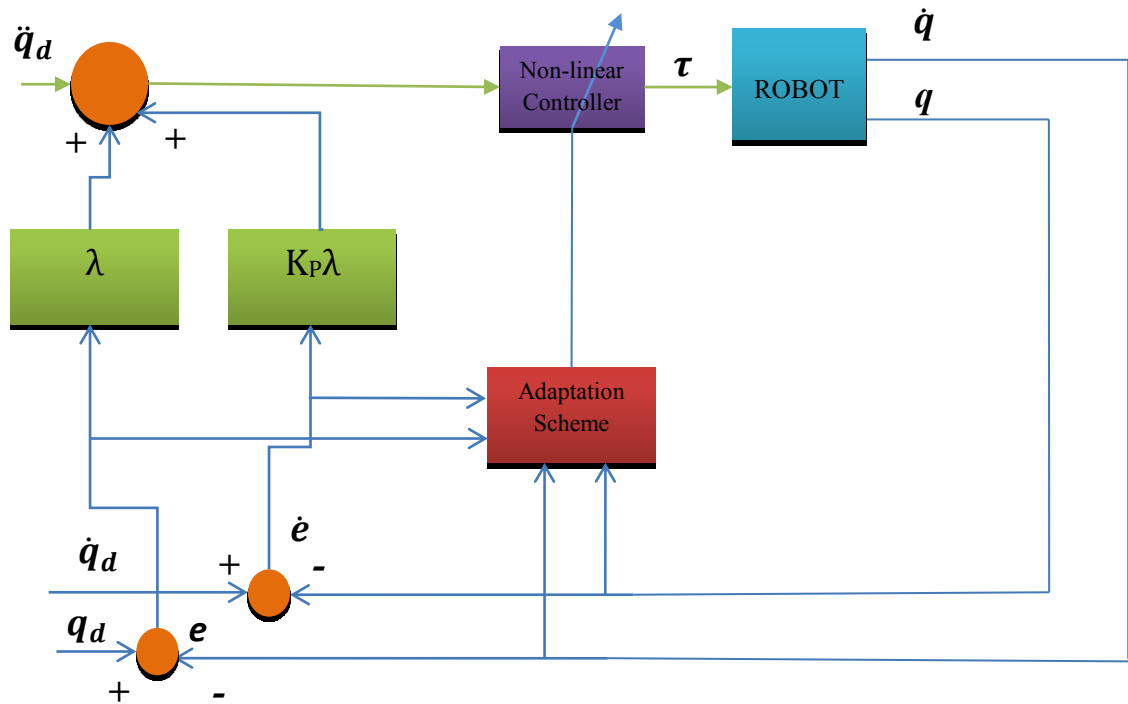


Figure 18. Control architecture for adaptive algorithm

Adaptive algorithm is a comprehensively researched concept which aims at minimizing the error between predicted and actual parameters of the system. This method provides a strategy which is sensitive to un-modeled dynamics and attempts to cater these by keeping track of the difference between desired and actual trajectories, updating parameters to minimize the resultant error.

The version of the algorithm used in this thesis was presented by Slotine and Li [51], with their introduction of a sliding variable to the original concept of a passivity based controller. Passivity based controllers originate from the idea of shifting the energy minimum of the system from,

$$(q, \dot{q}) = (0,0) \gg (e, \dot{e}) = (0,0)$$

thus ensuring that the potential energy and the kinetic energy of the system goes to zero [52]. The overall structure of this technique is shown in Figure 18.

A sliding variable which ensures global and asymptotic stability of the system, is defined as,

$$r = \dot{e} + \lambda e \tag{11}$$

$$e = q_d - q \tag{12}$$

$$\dot{e} = \dot{q}_d - \dot{q} \tag{13}$$

which implies that if $r \rightarrow 0$, then $e \rightarrow 0$ as $t \rightarrow \infty$. The new reference trajectory is defined as,

$$q_r = q_d - \lambda \int e dt \tag{14}$$

$$\dot{q}_r = \dot{q}_d - \lambda e \tag{15}$$

$$\ddot{q}_r = \ddot{q}_d - \lambda \dot{e} \tag{16}$$

In the equations above, q_r refers to new reference trajectory while q_d represents desired trajectory. The general equation of motion for the acrobot model is given as,

$$\tau = D(q)\ddot{q} + C(q, \dot{q})\dot{q} + F(\dot{q}) + G(q) \quad (17)$$

The update of parameters requires this equation to be rewritten in a parametric form where the respective matrices are defined as,

$$D(q) = \begin{bmatrix} (P_1 + P_2 + P_3 2 \cos(q_2)) & (P_2 + P_3 \cos(q_2)) \\ (P_2 + P_3 \cos(q_2)) & P_2 \end{bmatrix} \quad (18)$$

$$G(q) = \begin{bmatrix} -P_4 \cos(q_1) - P_5 \cos(q_1 + q_2) \\ -P_5 \cos(q_1 + q_2) \end{bmatrix} \quad (19)$$

$$C(q, \dot{q}) = \begin{bmatrix} P_3 \sin(q_2) \dot{q}_2^2 + 2P_3 \sin(q_2) \dot{q}_2 \dot{q}_1 \\ -P_3 \sin(q_2) \dot{q}_1^2 \end{bmatrix} \quad (20)$$

$$F(\dot{q}) = \begin{bmatrix} -P_6 \operatorname{sgn}(\dot{q}_1) - P_7 \dot{q}_1 \\ -P_8 \operatorname{sgn}(\dot{q}_2) - P_9 \dot{q}_2 \end{bmatrix} \quad (21)$$

The parameters in the above matrices are as follows,

$$\begin{aligned} P_1 &= m_1 l_{c1}^2 + m_2 l_1^2 + I_1 \\ P_2 &= m_2 l_{c2}^2 + I_2 \\ P_3 &= m_2 l_1 l_{c2} \\ P_4 &= (m_1 l_{c1} + m_2 l_1)g \\ P_5 &= m_2 l_{c2} g \\ P_6 &= f_{c1} \\ P_7 &= f_{v1} \\ P_8 &= f_{c2} \\ P_9 &= f_{v2} \end{aligned} \quad (22)$$

where m represents equivalent mass, l represents total length, l_i represents the length of link i between adjacent joints, l_{ci} defines distance between CoM of link i to the base of the respective joint, g represents acceleration due to gravity while f_c and f_v represent coulomb and viscous friction terms. The resultant update law is given by,

$$\tau = \Psi(q, \dot{q}, v, a)\hat{P} + K_P r \quad (23)$$

$$\hat{P} = -\Gamma^{-1}\psi^T(q, \dot{q}, \dot{q}_r, \ddot{q}_r)r \quad (24)$$

where $\psi^T(q, \dot{q}, \dot{q}_r, \ddot{q}_r)$ is the regressor matrix which represents model parameters in linear form and is a function of \dot{q}_r and \ddot{q}_r . \hat{P} determines the updated parameter values and Γ represents a constant positive definite matrix which is manually tuned to specify the rate of update for parameters. The adaptation law guarantees convergence of tracking errors [51]. However, it is essential to have a rough estimate of the dynamic parameters of the model so that the tuned parameters are only updated within a certain range.

4.3 Implementation

For parameter estimation, ASLAN has been trained by introducing simple sinusoidal trajectories with varying amplitude and frequencies. These trajectories serve as reference to be followed, while tuning parameters of the non-linear model. The final values obtained at the end of this experiment have been tabulated in Table 3.

Table3. Final parameters and gain values

PARAMETER	ESTIMATED	PARAMETER	ESTIMATED
\hat{P}_1	5.309	\hat{P}_7	-2.780
\hat{P}_2	0.802	\hat{P}_8	0.500
\hat{P}_3	1.510	\hat{P}_9	-23.50
\hat{P}_4	88.18	K_p	22.50
\hat{P}_5	26.45	λ	11.00
\hat{P}_6	0.200	$\Gamma_1 - \Gamma_9$	0.500

Here the parameters $\Gamma_1 - \Gamma_9$ make up the diagonal elements of the matrix Γ , while all non-diagonal elements are zero.

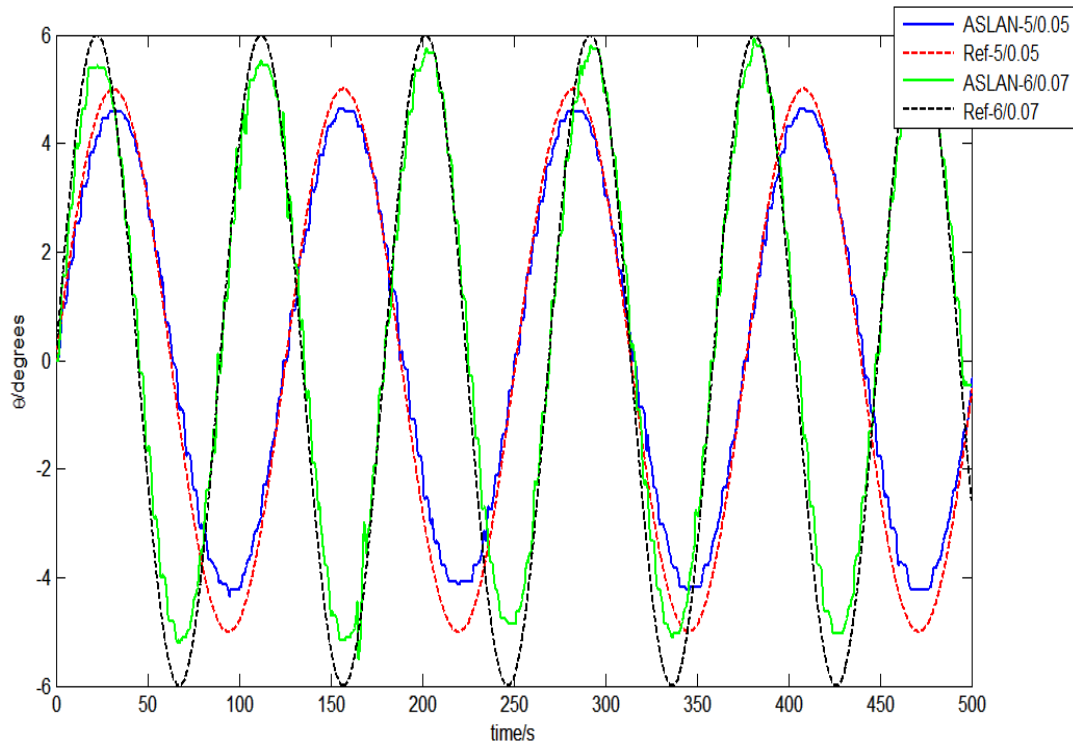
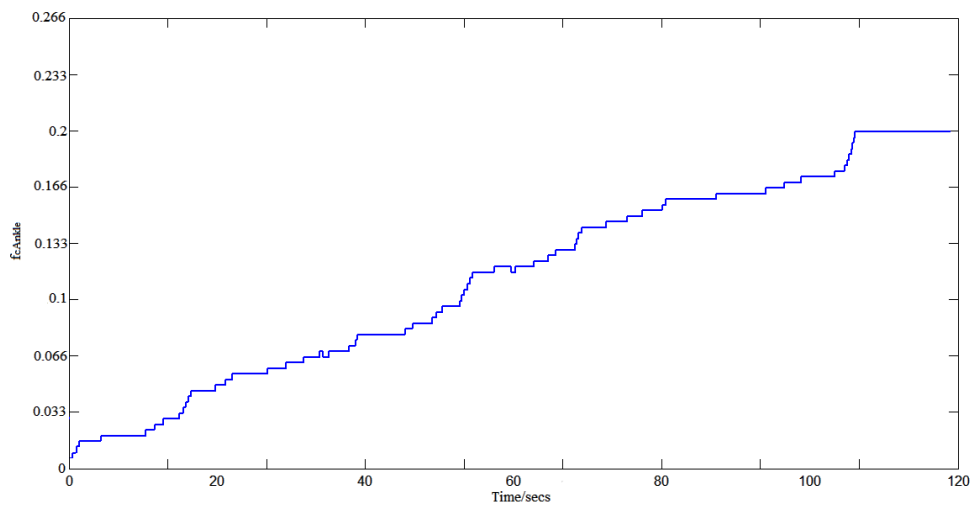
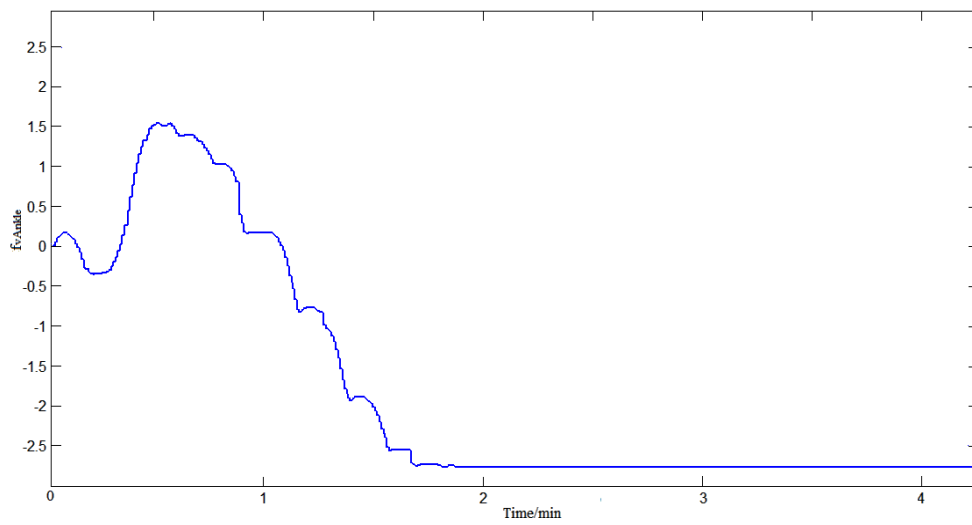


Figure19. Results for tracking reference trajectory after tuning parameters through Adaptive Control

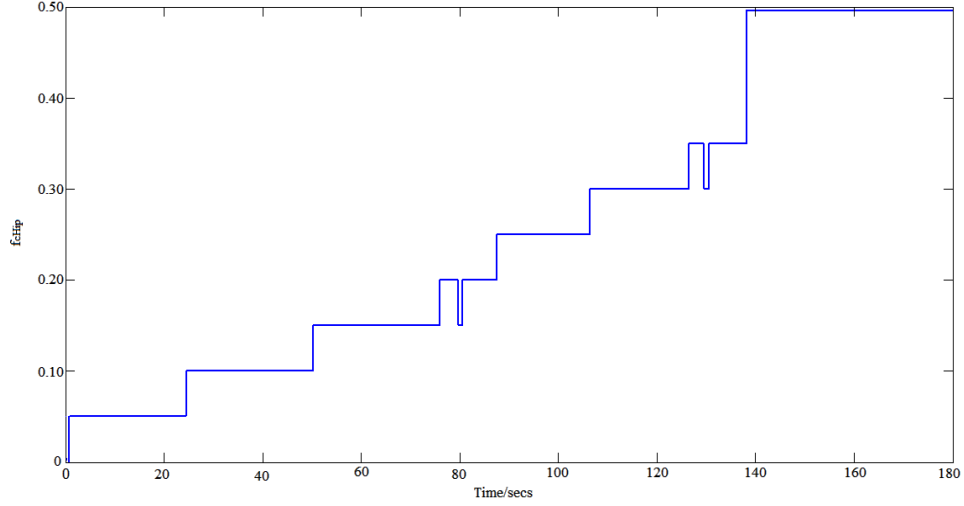
Results for sinusoidal trajectories with amplitudes of 3 and 6 degrees with an associated frequency of 0.5 and 0.7 Hz respectively, have been shown in figure 19. The graph reflects the accuracy of the final values of these parameters, which are used in the next section to design a non-linear controller for humanoid stabilization. This process allows estimation of parameters without going through the trouble of designing complex trajectories. Also the rate of convergence may be increased by varying the gain K_P and λ .



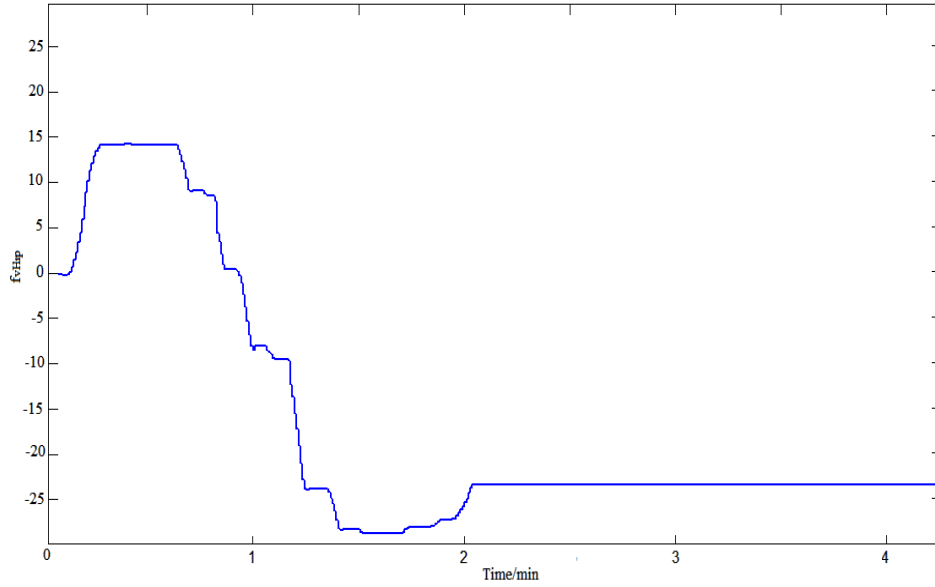
a) P_6 convergence through adaptive tuning
b)



b) P_7 convergence through adaptive tuning



c) P_8 convergence through adaptive tuning



d) P_9 convergence through adaptive tuning

Figure20. Results for parameter convergence through Adaptive Control

The figures above show how convergence is achieved for friction model parameters, $P_6 - P_9$ respectively, where initial values were chosen to be zero. For parameters $P_1 - P_5$, initial values were extracted from CAD drawings, which showed slight variation, of three significant figures, after adaptive tuning. Thus the final values were kept unchanged for these parameters.

The complete non-linear model takes the following form,

$$\Psi(q, \dot{q}, v, a) \hat{P} = \tau \quad (25)$$

where $\Psi(q, \dot{q}, v, a)$ is a 2×9 matrix and its coefficients are defined as,

$$\Psi_{11} = \ddot{\theta}_1$$

$$\Psi_{12} = (\ddot{\theta}_1 + \ddot{\theta}_2)$$

$$\Psi_{13} = (2 \cos(q_2) \ddot{\theta}_1 + \cos(q_2) \ddot{\theta}_2 - \sin(q_2) \dot{q}_2^2 - 2 \sin(q_2) \dot{q}_2 \dot{q}_1)$$

$$\Psi_{14} = \cos(q_1)$$

$$\Psi_{15} = \cos(q_1 + q_2)$$

$$\Psi_{16} = \text{sign}(\dot{q}_1)$$

$$\Psi_{17} = \dot{q}_1$$

$$\Psi_{18} = 0$$

$$\Psi_{19} = 0$$

$$\Psi_{21} = 0$$

$$\Psi_{22} = (\ddot{\theta}_1 + \ddot{\theta}_2)$$

$$\Psi_{23} = \cos(q_2) \ddot{\theta}_1 + \sin(q_2) \dot{q}_1^2$$

$$\Psi_{24} = 0$$

$$\Psi_{25} = \cos(q_1 + q_2)$$

$$\Psi_{26} = 0$$

$$\Psi_{27} = 0$$

$$\Psi_{28} = \text{sign}(\dot{q}_2)$$

$$\Psi_{29} = \dot{q}_2$$

Thus the final extracted model is defined in parametric terms, which represents inertial properties of the complete humanoid robot in an aggregated form.

4.4 Summary

This chapter introduces the acrobot model to represent the simplified dynamics of the complete humanoid robot. Adaptive algorithm was used to estimate parameters for this simplified model. The aim was to extract a non-linear system which captures the dynamics of the complex humanoid structure, in a sagittal plane only. This model will facilitate in formulation of the balancing control strategy, as described in chapter 5.

Chapter 5

Linear Control Design

In order to resolve the problem of stabilization, linear state feedback is the simplest control approach which may be employed. This controller is designed based on linearization of the non-linear model extracted in chapter 4. For this purpose, the non-linear equations of the system are linearized around q_{1D}^* , q_{2D}^* , which represents the desired position for the system for stabilization. The state x for linearization is defined as,

$$x = [q_1, q_2, \dot{q}_1, \dot{q}_2]^T, \quad (26)$$

$$\mathbf{q} = [q_1, q_2]^T, \quad \dot{\mathbf{q}} = [\dot{q}_1, \dot{q}_2]^T, \quad (27)$$

Where q_1 and q_2 represent angular rotations for ankle and hip respectively, while \dot{q}_1 and \dot{q}_2 represent respective angular velocities. The process of linearization is determined by employing Taylor series expansion, evaluated around the equilibrium point, as follows,

$$\dot{x} = f(x, u) \approx f(x^*, u^*) + \left[\frac{\partial f}{\partial x} \right]_{x=x^*} (x - x^*) + \left[\frac{\partial f}{\partial u} \right]_{x=x^*, u=u^*} (u - u^*) \quad (28)$$

This expansion evaluates the differential of the non-linear function, with respect to the state variable x and control input u . the resultant state space model is determined by,

$$\dot{x} = Ax + Bu \quad (29)$$

Such that matrices A and B are defined as follows:

$$A = \left[\frac{\partial f}{\partial x} \right]_{x=x^*} \quad B = \left[\frac{\partial f}{\partial u} \right]_{u=u^*} \quad (30)$$

The matrix A encapsulates the dynamical properties of the system that exist due to the particular chosen state, while B determines the effect an input will have on the respective states.

The idea of linearization around the equilibrium state represents a simplified model which is only valid within a close vicinity to this point. Thus the underlying assumption for this control technique implies instability for large deviations from the desired position.

5.1 Linearization of Non-Linear Model

The complete non-linear model extracted from parameter estimation in the previous section consists of dynamic parameters of the model, in terms of inertial properties, friction parameters and controller gains. The reason behind using the complete non-linear model for linearization is an attempt to have representation of all properties that play a role in determining the dynamics of the actual system.

Linearization involves evaluation of the nonlinear function at the equilibrium point, which simplifies and decouples the system for control purposes. The non-linear model, to be linearized, is given in its parametric form in Equation 25, which can be rewritten such that the components of the equation are divided into inertial,

gravitational, coriolis and frictional components (from chapter 4). The properties are represented by the matrices H , G , C , F and K respectively.

$$H \begin{bmatrix} \ddot{q}_1 \\ \ddot{q}_2 \end{bmatrix} = \tau + C + G + F \quad (31)$$

Where the matrices can be written as follows,

$$H = \begin{bmatrix} (P_1 + P_2 + P_3 \cos(q_2)) & (P_2 + P_3 \cos(q_2)) \\ (P_2 + P_3 \cos(q_2)) & P_2 \end{bmatrix}$$

$$G = \begin{bmatrix} -P_4 \cos(q_1) - P_5 \cos(q_1 + q_2) \\ -P_5 \cos(q_1 + q_2) \end{bmatrix}$$

$$C = \begin{bmatrix} P_3 \sin(q_2) \dot{q}_2^2 + 2P_3 \sin(q_2) \dot{q}_2 \dot{q}_1 \\ -P_3 \sin(q_2) \dot{q}_1^2 \end{bmatrix}$$

$$F = \begin{bmatrix} -P_6 \text{bipolar}(\dot{q}_1) - P_7 \dot{q}_1 \\ -P_8 \text{bipolar}(\dot{q}_2) - P_9 \dot{q}_2 \end{bmatrix}$$

Linearization of this non-linear model is carried out by differentiation of individual matrices with respect to the state x and control input u which is torque commanded to the actuators represented by τ . The final linearized equation is defined by the following equation:

$$\dot{x} = \begin{bmatrix} 0_{2 \times 2} & I_{2 \times 2} \\ -D^{-1} \frac{\partial G}{\partial q} & -D^{-1} \frac{\partial F}{\partial \dot{q}} \end{bmatrix} \begin{bmatrix} q_1 \\ q_2 \\ \dot{q}_1 \\ \dot{q}_2 \end{bmatrix} + \begin{bmatrix} 0 \\ D^{-1} B \end{bmatrix} \begin{bmatrix} \tau_A \\ \tau_H \end{bmatrix} \quad (32)$$

where the matrix B is evaluation of the differential of function with respect to τ and is given as ,

$$B = \begin{bmatrix} 0 & 0 \\ 0 & 1 \end{bmatrix}$$

while the differential of other matrices with respect to the state x are given as,

$$\frac{\partial G}{\partial q} = \begin{bmatrix} P_4 \sin(q_1) + P_5 \sin(q_1 + q_2) & P_5 \sin(q_1 + q_2) \\ P_5 \sin(q_1 + q_2) & P_5 \sin(q_1 + q_2) \end{bmatrix}$$

$$\frac{\partial C}{\partial \dot{q}} = \begin{bmatrix} 2P_3 \sin(q_2) \dot{q}_2 & \sin(q_2) 2P_3 \dot{q}_2 + 2P_3 \sin(q_2) \dot{q}_1 \\ -\sin(q_2) 2P_3 \dot{q}_1 & 0 \end{bmatrix}$$

$$\frac{\partial F}{\partial \dot{q}} = \begin{bmatrix} -P_6 \frac{\alpha}{2 \cosh \left(\left(\frac{\alpha * \dot{q}_1}{2} \right)^2 \right)} - P_7 & 0 \\ 0 & -P_8 \frac{\alpha}{2 \cosh \left(\left(\frac{\alpha * \dot{q}_2}{2} \right)^2 \right)} - P_9 \end{bmatrix}$$

The matrices G, C, F and H^{-1} evaluated at the equilibrium point $x = [1.57, 0, 0, 0]$ are defined as,

$$G_{x=x^*} = \begin{bmatrix} P_4 + P_5 & P_5 \\ P_5 & P_5 \end{bmatrix}$$

$$C_{x=x^*} = \begin{bmatrix} 0 & 0 \\ 0 & 0 \end{bmatrix}$$

$$F_{x=x^*} = \begin{bmatrix} -P_6 \frac{\alpha}{2} - P_7 & 0 \\ 0 & -P_8 \frac{\alpha}{2} - P_9 \end{bmatrix}$$

$$H^{-1}_{x=x^*} = \begin{bmatrix} (P_1 + P_2 + 2P_3) & (P_2 + P_3) \\ (P_2 + P_3) & P_2 \end{bmatrix}^{-1}$$

After linearization, it can be seen that coriolis and centrifugal terms extant in the original equations have been eliminated and do not contribute to the simplified model. However, all other dynamic properties of the original system represent themselves in the linearized form, retaining essence of the true dynamics to a certain extent.

Having defined the state space model, it is important to determine appropriate control input which will guarantee stability and convergence of the system to the desired position. For this purpose, state feedback is employed which requires gain tuning to get convergence at the desired rate, under constraints imposed by actuator and joint limitations. Optimality in this situation is determined by employing the linear quadratic regulator, described in the next section.

5.2 Linear Quadratic Regulator-The Theory

In order to determine the optimal trajectory, after the push, towards the vertical desired position, an optimal feedback controller needs to be designed. Optimality [4] has been defined in terms of a quadratic cost function as follows,

$$J = \frac{1}{2} \int_0^{\infty} (x^T Q x + u^T R u) dt \quad (33)$$

$$Q = Q^T > 0, R = R^T > 0$$

The linear feedback matrix u is defined as,

$$u = -Lx \quad (34)$$

The L matrix is responsible for defining optimality in the linear quadratic regulator.

This matrix is obtained by solving the riccati equation which is given as follows,

$$A^T P + PA - PBR^{-1}B^T P + Q = 0 \quad (35)$$

The gain matrix is determined by,

$$L = R^{-1}B^T P \quad (36)$$

By varying the gain matrices Q and R , the penalty on error of the state x and the control effort u is controlled. The gain matrices used in experimentation are,

$$Q = \begin{bmatrix} 1 & 0 & 0 & 0 \\ 0 & 1 & 0 & 0 \\ 0 & 0 & 1 & 0 \\ 0 & 0 & 0 & 1 \end{bmatrix}, \quad R = 10e - 12$$

where a higher penalty is placed on the control effort as compared to the state. These gains are determined by keeping in mind joint motor limitations for providing the control effort in terms of torque. This approach is much faster as compared to traditional pole placement techniques, while the desired balance of priorities between the state and control effort can be regulated much easily.

5.3 Simulation Results in MATLAB

The resultant state space model, derived in the section above, is tested under disturbance applied to the system. Controller gains for the resultant feedback controller are as follows,

$$L = [-774.5 \quad 456.2 \quad -181.4 \quad 10.04]$$

Figure 21 shows convergence has been achieved within an approximate duration of 4 seconds, but the control effort employed goes up to - 10 amperes, which is quite out of reach for the actuators. If the R gain value is increased, to employ lower control effort, stabilization is achieved after a few oscillations, as shown in Figure 22.

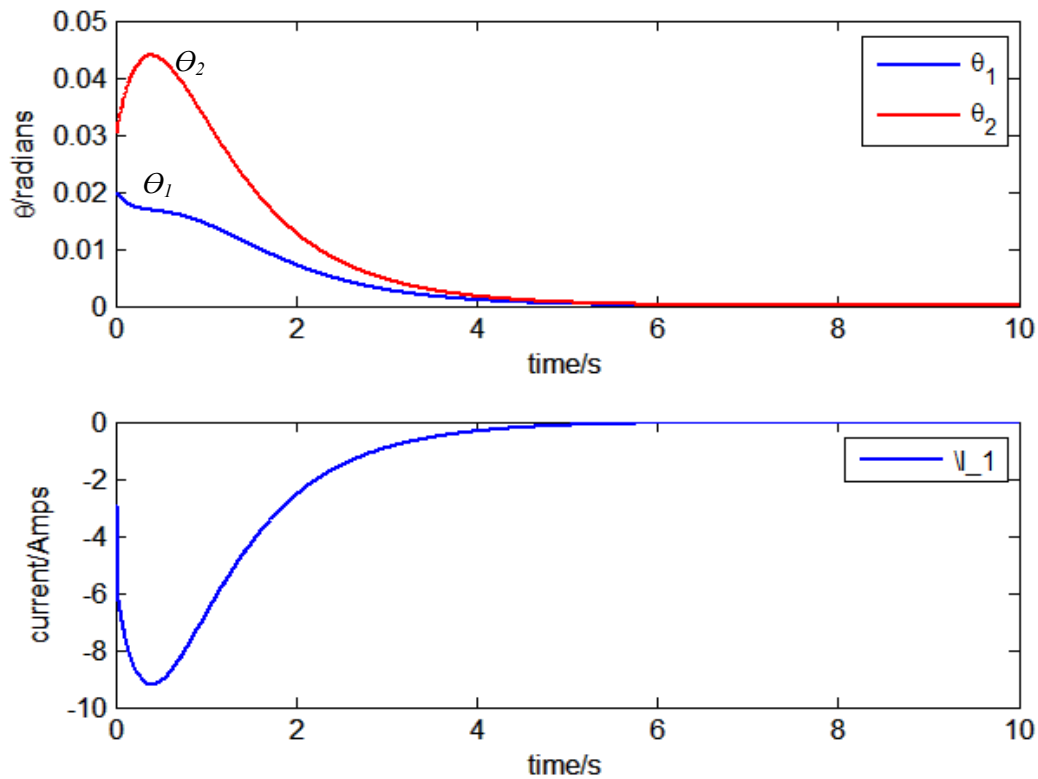


Figure 21. Simulation results for $x_0 = [0.02; 0.03; 0; 0]$

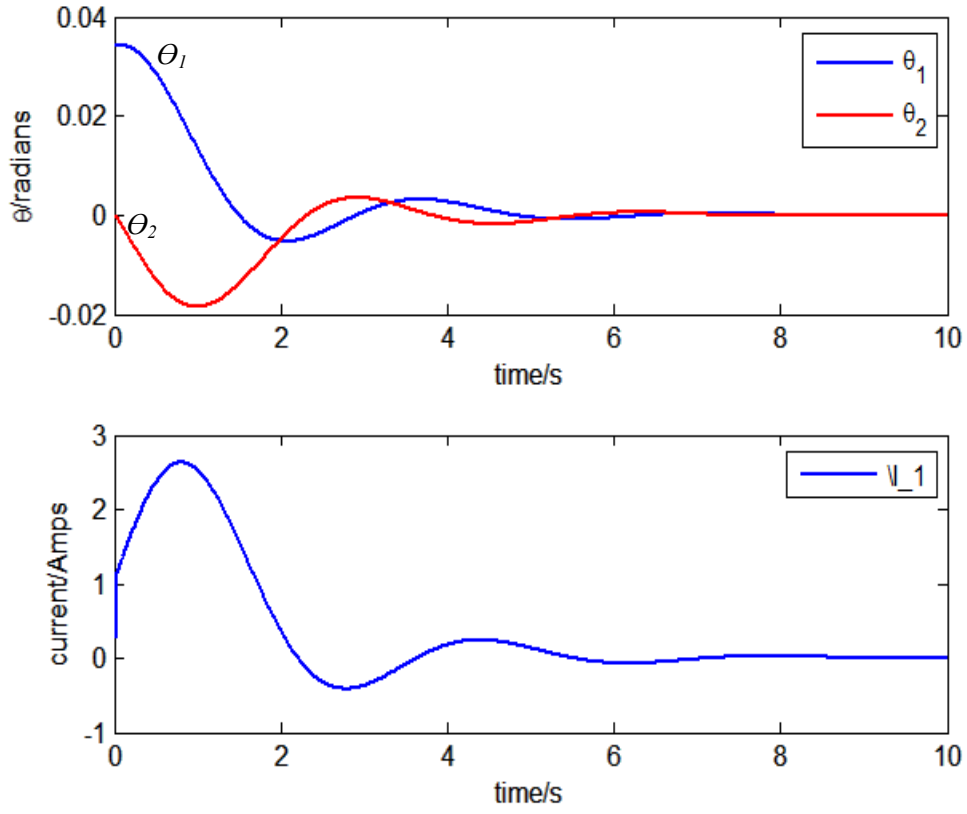


Figure 22. Simulation results $x_0 = [0.02; 0.03; 0; 0]$ with higher R value

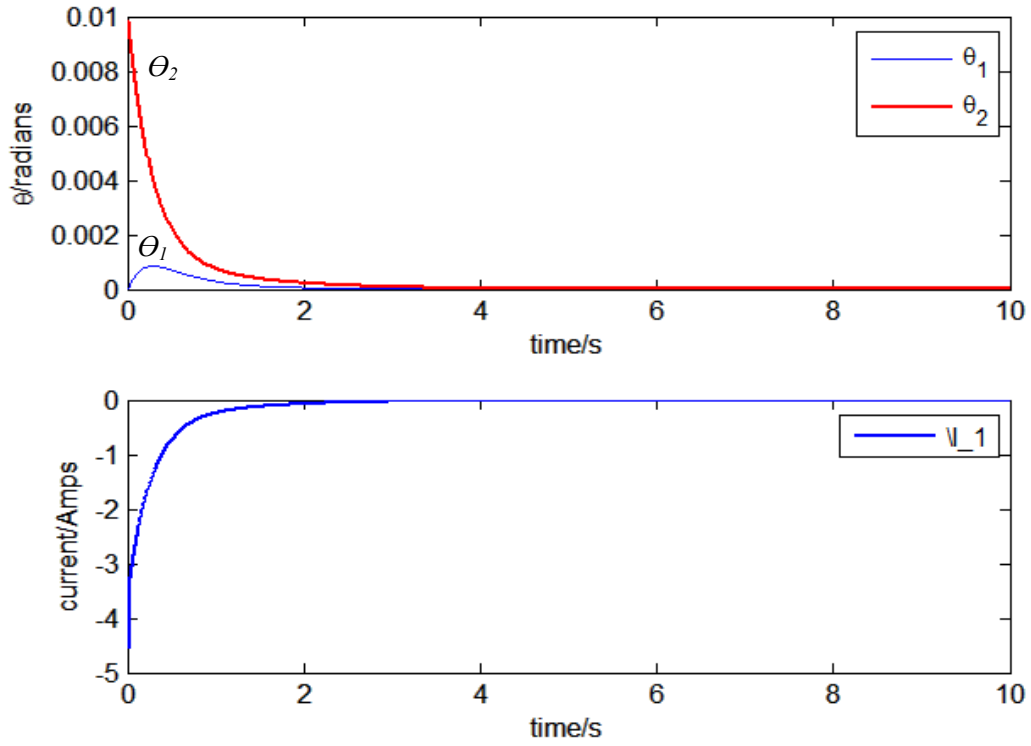


Figure 23. Simulation results $x_0 = [0; 0.01; 0; 0]$ for upper body disturbance only

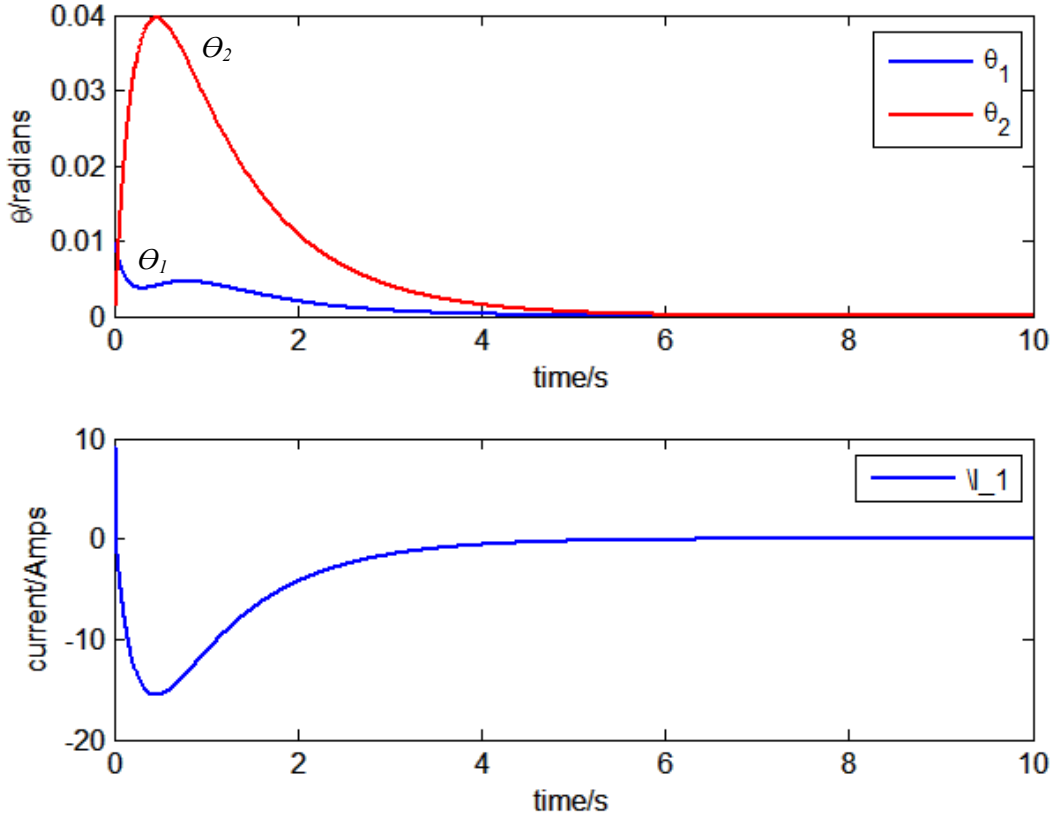


Figure 24. Simulation results $x_0 = [0.01; 0; 0; 0]$ for lower body disturbance only

Figures 23 and 24 show that if only a disturbance in the hip joint is induced, the desired current remains within range. However, desired control effort goes out of range if only ankle joint disturbance is induced. Since the humanoid is modeled as an acrobot, it is inevitable to push the robot in a way which causes only hip joint instability. Thus this approach is not suitable when passive ankle joint stabilization is required.

5.4 Summary

The results show that the current required to stabilize the system without oscillation is greater than the DC motor limit at the hip. Experimentation also shows that a push

causing disturbance in the upper body only did not require current that was out of range for the motors, which is essentially not possible since any disturbance to the system would affect both ankle and hip joints. Also, a slight disturbance in the ankle joint immediately requires greater control effort for stabilization.

Chapter 6

Partial Feedback Linearization

In the last chapter a linear feedback controller was designed using LQR. The drawback of employing this technique is requirement of higher control effort than the actuator limitation. This problem is evident during stabilization of the passive ankle joint. Therefore, a non-linear control approach is adopted with the aim of stabilizing the ankle, employing control effort within actuators limits.

6.1 Partial Feedback Linearization- the Theory

Since the bipedal robot has been modeled as an under-actuated system, with passive ankle and active hip joints, it is essential to comprehend that such systems are not completely feedback linearizable. This section of the thesis introduces '***Partial Feedback Linearization***' control which is based on linearizing the actuated degree of freedom, by introducing non-linear feedback in the control loop. This methodology is quite common when it comes to the control of autonomous manipulators, but is not generally approached for bipedal robots. A huge contributing factor is the ignorance of the true non-linearities of the complete system, which is difficult to articulate independently for each limb. Hence, parameter estimation through adaptive control remains of vital importance to the implementation of this controller.

The objective of a partial feedback linearization controller is to employ the nonlinear model as feedback to be able to nullify the non linearities and create a resultant linear system to control. This approach has been implemented by Spong [50], in two ways, namely *Collocated* and *Non Collocated* linearization.

Collocated, as the name suggests, is a control strategy to control the actuated link in an acrobot, essentially the upper body. Non-Collocated linearization provides the capacity to control the passive or un-actuated link in the system, which in our case is the ankle joint of the humanoid robot. Since the objective of employing non-linear feedback is to stabilize the ankle, Non-Collocated Partial Feedback Linearization (NCPFL) is employed. Proceeding sections of this chapter highlight the technicalities behind implementation of this control technique.

6.2 Non-Collocated Partial Feedback Linearization (NCPFL)

In contradiction to Collocated linearization, *Non-Collocated partial feedback linearization* involves the direct control of the passive joint, employing upper body movements through hip joint actuation. This control strategy may be implemented given the condition defined by *Strong-Inertial Coupling* [38]. This condition imposes restrictions on the inertia matrix of the system stating,

$$\text{rank}(d_{12}(q)) = n - m \quad (37)$$

where n is the total number of degrees of freedom, m refers to the actuated number of degrees of freedom, d_{12} is the coefficient described in equation 1. This condition

requires that the number of active degrees of freedom should be greater or equal to the number of passive joints in the system.

Since this condition is satisfied by the chosen acrobot model, the nonlinear feedback controller is designed such that the output to be controlled is the angle of the ankle joint, reducing its dynamics to a second order linear system,

$$y = q_1 \quad (38)$$

Considering the following equations of motion derived from equation 1 and 2, yields the following non-linear model,

$$d_{11}\ddot{q}_1 + d_{12}\ddot{q}_2 + G_1 + C_1 + F_1 = 0 \quad (39)$$

$$d_{21}\ddot{q}_1 + d_{22}\ddot{q}_2 + G_2 + C_2 + F_2 = \tau_{hip} \quad (40)$$

Manipulation of Equation 39 with an assumption of no ankle torque leads to,

$$\ddot{q}_2 = -d_{12}^{-1}(d_{11}\ddot{q}_1 + G_1 + C_1 + F_1) \quad (41)$$

Substituting Equation 41 in Equation 40 yields the following expression,

$$\tilde{M}_{21}v_1 + \tilde{C}_2 + \tilde{G}_2 + \tilde{F}_2 = \tau \quad (42)$$

Such that

$$\tilde{M}_{21} = d_{21} - d_{22}d_{12}^{-1}d_{11}$$

$$\tilde{C}_2 = C_2 - d_{22}d_{12}^{-1}C_1$$

$$\tilde{G}_{21} = G_2 - d_{22}d_{12}^{-1}G_1$$

$$\tilde{F}_2 = F_2 - d_{22}d_{12}^{-1}F_1$$

These terms expressed in parametric form extracted from chapter 4 yields the following expressions respectively,

$$\tilde{M}_{21} = (P_2 + P_3 \cos(q_2)) - P_2 \frac{-P_1 + P_2 + 2P_3 \cos(q_2)}{(P_2 + P_3 \cos(q_2))}$$

$$\tilde{C}_2 = \frac{P_2(P_3 \sin(q_2) \dot{q}_2^2 + 2P_3 \sin(q_2) \dot{q}_2 \dot{q}_1)}{(P_2 + P_3 \cos(q_2))} + P_3 \sin(q_2) \dot{q}_1^2$$

$$\tilde{G}_2 = \frac{P_2(-P_4 \cos(q_1) - P_5 \cos(q_1 + q_2))}{(P_2 + P_3 \cos(q_2))} + P_5 \cos(q_1 + q_2)$$

$$\tilde{F}_2 = \frac{P_2(-P_7 \dot{q}_1 - P_6 \text{bipolar}(\dot{q}_2))}{(P_2 + P_3 \cos(q_2))} + P_8 \text{bipolar}(\dot{q}_2) + P_9 \dot{q}_2$$

Since the objective is to restore q_l to its equilibrium state of $q_l^* = 90^\circ$, which represents a vertical configuration for the lower body, the following additional control input is added,

$$v_1 = \ddot{q}_1 \tag{43}$$

which is replaced by local PD control terms as follows,

$$v_1 = -K_{vD} \dot{q}_1 + K_{vP} (1.57 - q_1) \tag{44}$$

This input effectively reduces the dynamics of the lower link to a second order linear system. Local stability properties of this controller are explained and verified in [50].

6.3 Simulation Results in MATLAB

The performance of this controller has been tested in MATLAB. The gain values used for NCPFL are $K_{vD} = -30$, and $K_{vP} = -5$, which are manually tuned values. Employing these gains, the response of this system, to an initial disturbance of approximately 1.2 degrees to the ankle and 1.7 degrees to the hip, responds in the manner shown in Figure 25.

The graph below shows convergence has been achieved with an approximate duration of 4 seconds, but the control effort employed goes up to -6 amperes, which is within the prescribed limits for the actuators.

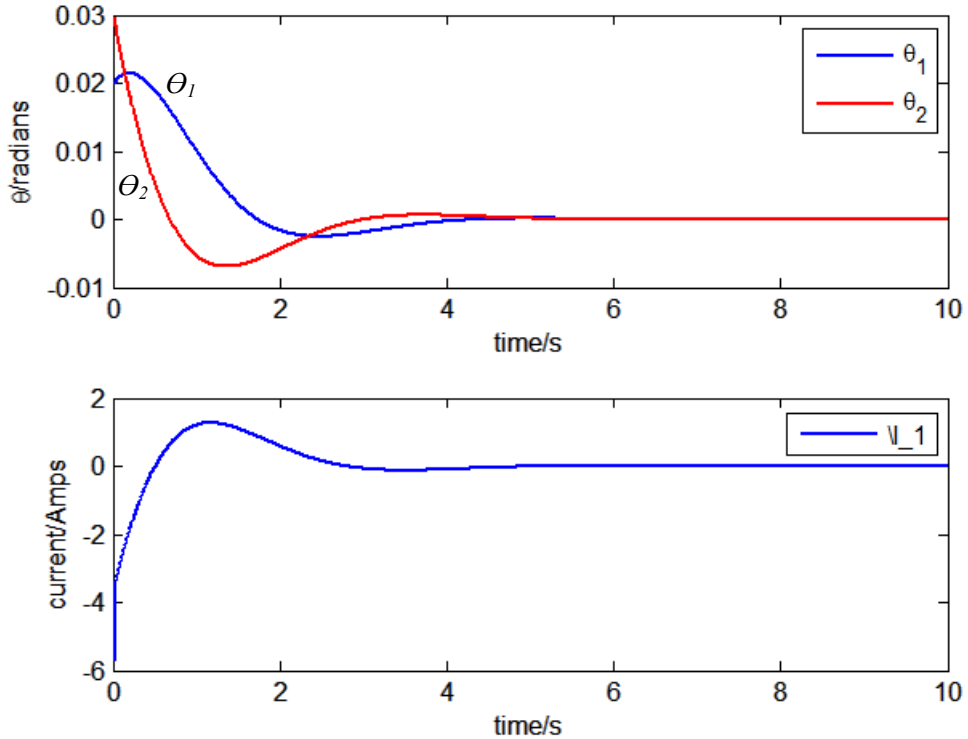


Figure 25. Simulation results $x_0 = [-0.02; 0.03; 0; 0]$ using NCPFL and LQR

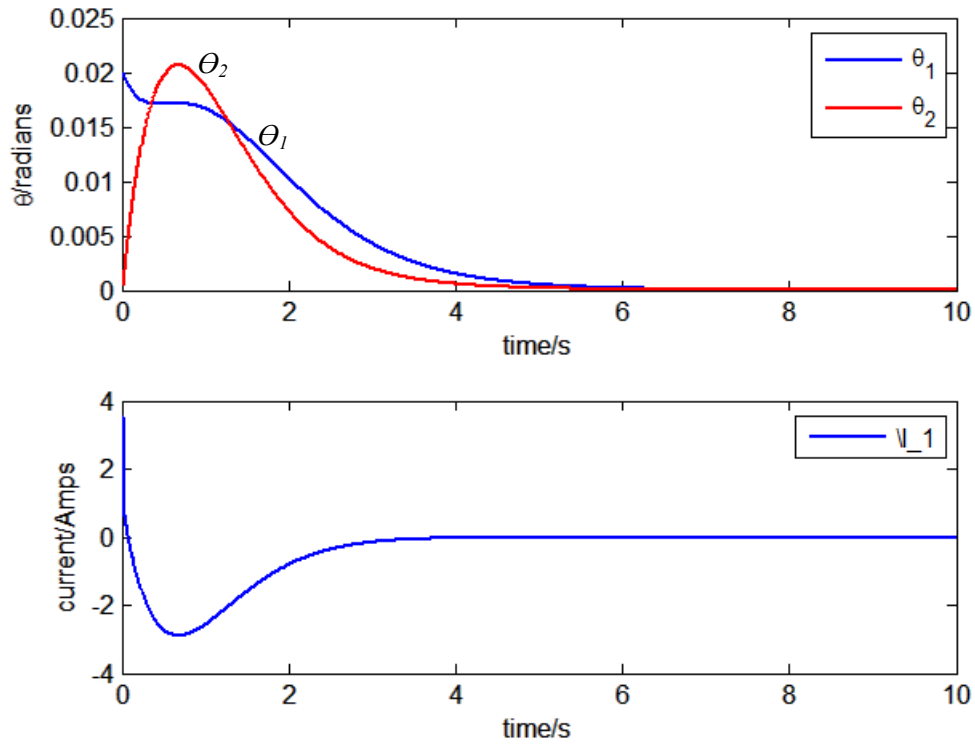


Figure 26. Simulation results $x_0 = [0.02; 0; 0; 0]$ using NCPFL

Figure 26 is another example of the response of NCPFL to a disturbance of 1.2 degrees in the lower body only, which results in a control effort requirement of up to -3amperes.

6.4 Summary

Experimentation shows that this control approach is apt for passive ankle stabilization. In order to achieve quick convergence for the hip joint, the linear feedback approach introduced in chapter 5, is integrated with NCPFL, only when the system is in a close vicinity to the equilibrium state. Details of implementation of this integrated approach have been described in the next chapter, followed by simulation verification in Webots and hardware experimentation.

Chapter 7

Full Body Control Architecture

Upon application of a push, the robot rotates about its feet, as a rigid structure, due to high friction at the hip joint. In order to stabilize the system using a single actuated degree of freedom at the hip, design of a non-linear control strategy for the derived model is explored. The controller described aims to stabilize the ankle of the biped as a first priority, which in turn leads to convergence of the hip joint near the desired state. However, during practical implementation, NCPFL may lead to oscillations of upper body before complete stabilization, due to which the system switches to a linear feedback controller, which swiftly stabilizes the humanoid.

Based on these objectives, the design of a synergy of linear and non-linear control strategy for the derived model has been explored. It has been seen from experimentation results in the previous chapters that a standalone linear state feedback controller was not able to cater lower body disturbance. Thus a non-linear approach has been adopted which caters this objective. The controller synergy is described in detail in the following section.

7.1 Full Body Control

A control hierarchy shown in Figure 27, has been designed to implement push recovery in real time. At every sampling time, the state x , including angular rotations

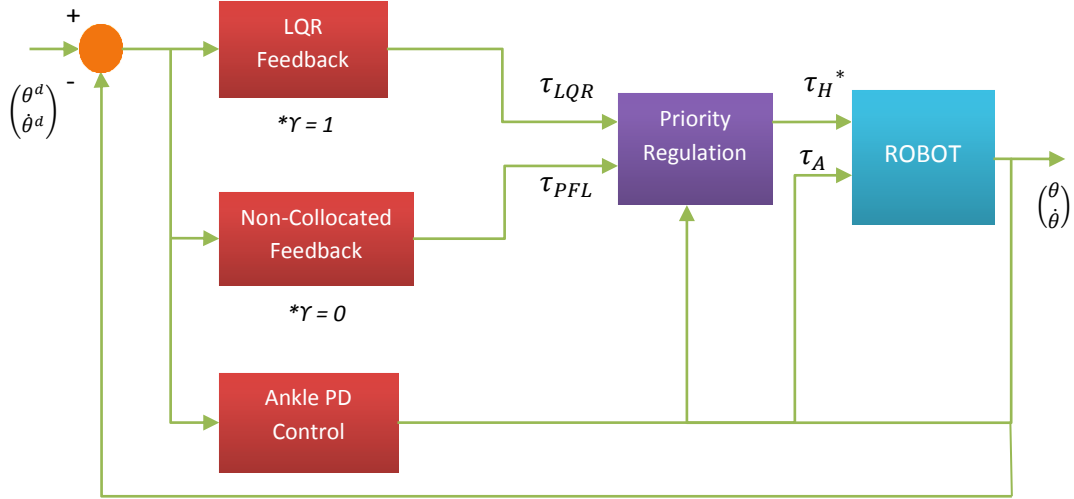


Figure 27. Full body control architecture

and velocities for ankle and hip, is estimated through motor encoders and IMU readings.

Locations of CoM_A and CoM_H (horizontal projections of ankle and hip joint angular displacements) of the chosen model determine which controller should be given priority over the other. Since upon application of push, CoM_A and CoM_H both are disturbed, the non-linear approach is employed. Once the lower body has converged to the desired state, while upper body is in close vicinity, linear feedback kicks in. Based on the boundary conditions defined below, a variable γ is introduced such that the value of γ is determined by,

$$\gamma = 0 \{ CoM_A > 0.01 \parallel CoM_A < -0.01 \} \quad (45)$$

$$\gamma = 1 \begin{cases} -0.01 < CoM_A < 0.01 \\ CoM_H > 0.005 \parallel CoM_H < -0.005 \end{cases} \quad (46)$$

The final torque value commanded to the motor is given by the following,

$$\tau_H^* = \tau_{PFL}(1 - \gamma) + \tau_{LQR}\gamma \quad (47)$$

The control strategy formulated defines desired torque for the hip joint. This is accompanied with a simple PD controller at the ankle which is given as,

$$\tau_A = K_{PA} (1.57 - q_1) - K_{DA}\dot{q}_1 \quad (48)$$

This ankle torque is employed to cater the friction components at the ankle joint. Since the assumption of ankle joint being passive cannot be achieved in a harmonic drive driven joint of the humanoid robot ASLAN, a small amount of torque is employed which assists in overcoming friction at the ankle joint to achieve desired control. It will be shown in experimental evaluation that desired ankle torque is greatly reduced with respect to available saturation levels of the actuator. Also, the effects of using the proposed controller as a standalone strategy, with effectively zero ankle torque, will be discussed in the preceding sections.

7.2 Implementation on WEBOTS

7.2.1 Simulation Setup

Detailed testing of the proposed strategy has been carried out in the Webots simulator [53]. The humanoid model of a humanoid robot shown in Figure 28, has been designed in this environment with a total length of 1.7m and weight of 86.6Kg. Each limb of the humanoid consists of six degrees of freedom. The robot consists of 3-axis

global positioning sensor (GPS) and 3-axis accelerometer for position and orientation sensing. The simulation and controller output is updated at a frequency of 125Hz.

The humanoid robot initially stands straight on an even terrain, and is eventually pushed to add disturbance to the stable system. The robot is pushed using an autonomous “ball” robot model which has a mobile base. This ball is equipped with a force sensor which measures the impulse at impact with the humanoid.



Figure 28. Humanoid Simulation Model in Webots

The height of the ball is at 1.2m such that the humanoid robot is pushed in the middle of the torso. The ball does not apply a continuous push, but rather provides an impulse at the instant of collision. After impact, the robot driving the ball moves in an opposing direction and does not come into contact with the robot.

7.2.2 Implementation Details

The servos of the robot are operated in torque control mode, where the commanded torque is determined by equation 10. The gain values used for NCPFL are $K_{vD} = -30$, and $K_{vP} = -5$. The LQR controller is tuned in MATLAB where the values for Q and R matrices for state space model are given as $Q = I(4 \times 4)$ and $R = 10e^{-12}$. The optimized L matrix extracted is defined as $L = [30.15, 147.4, -25.29, -27.48]$. In this case, no PD controller is required at the ankle because Webots allows the servo motor to be operated in a torque mode which does not add any friction at the ankle joint.

With the parameters defined above, the simulation is tested under impulse of varying magnitude, imparted to the humanoid from both front and back, restricted to sagittal plane only. The variation in magnitude of this force is achieved by increasing the initial distance between the ball and the humanoid robot. The ball is controlled using an autonomous mobile base which moves in the direction towards the robot. At impact with the robot, detected by the force sensor in the ball, the direction of the base is reversed, creating an effect of a ball hitting the robot and bouncing back. An extra GPS is added at the location defined by CoM_{AVG} which is given as,

$$CoM_{AVG} = \frac{m_1 * CoM_A + m_2 * CoM_H}{m_1 + m_2} \quad (49)$$

This enables determination of CoM_{AVG} linear position and velocity. This term is primarily determined to extract phase plots for various trajectories and determine stable and unstable areas for the system.

7.3 Result Evaluation

Figure 29 shows the response of the humanoid robot under an instantaneous disturbance of 164Ns from the back. The graphs shown in Figure 30 reflect the ability of the controller to cater disturbances of such large magnitude. The graph also shows dependence of less than 10Nm on ankle torque while the saturation limits go much beyond this value. Figure 31 shows a similar response to 130Nm impulse imparted to the humanoid from the front while Figure 32 shows the resultant variation in angular rotation, CoM of each link and current employed by the actuators.

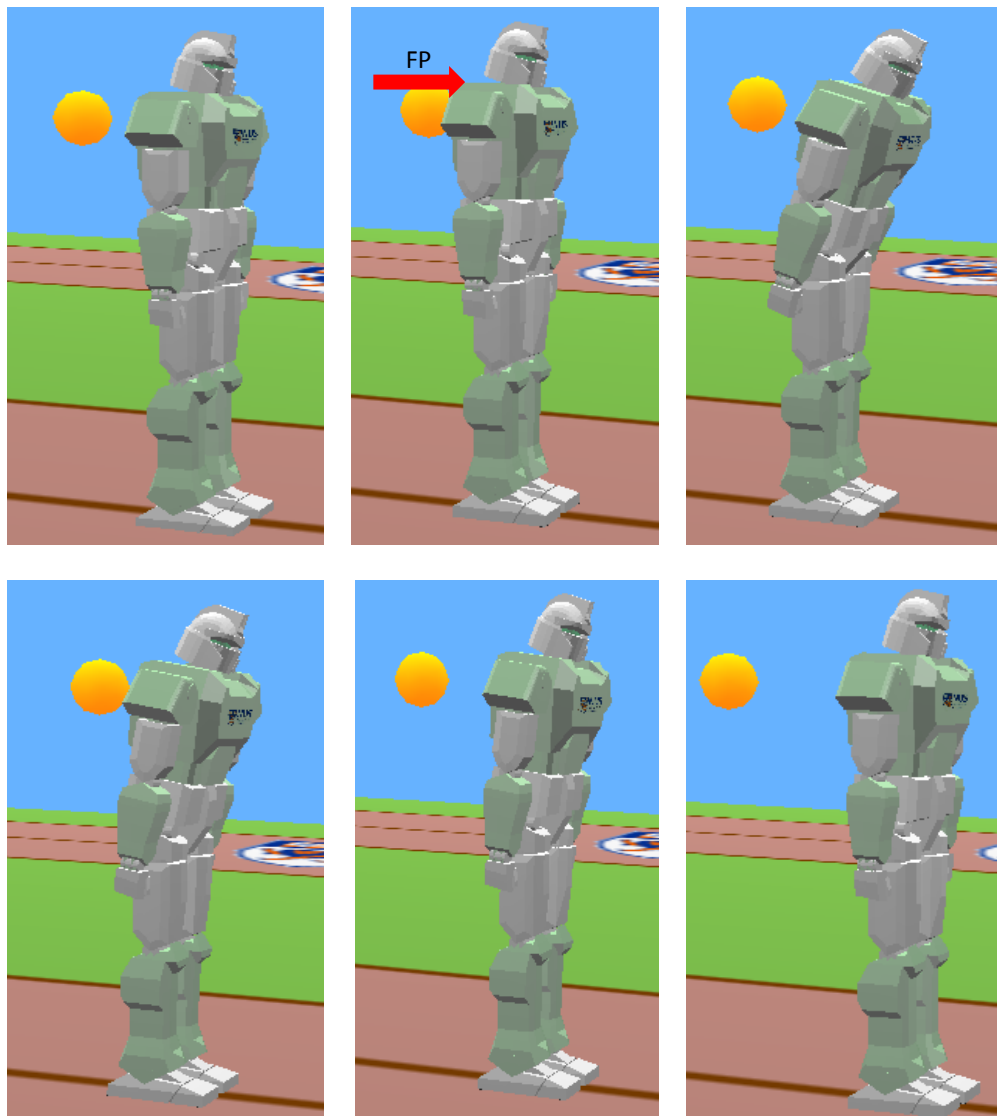
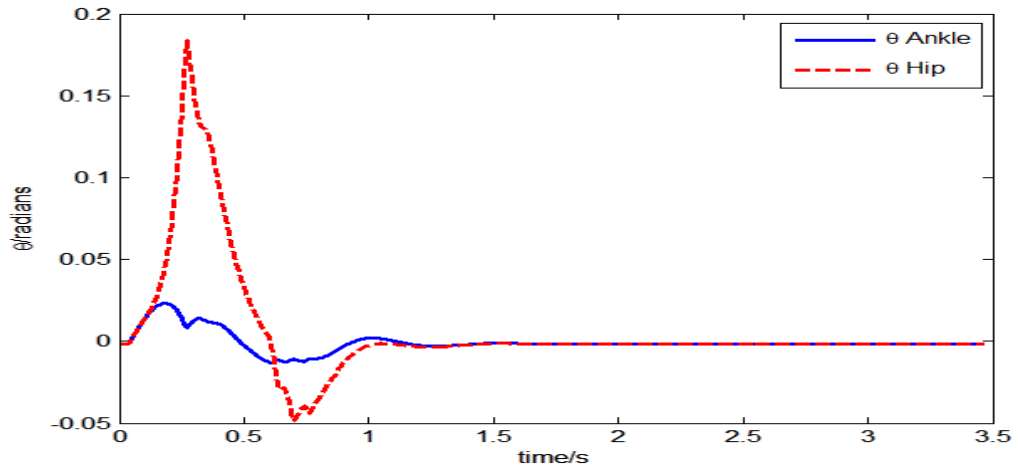
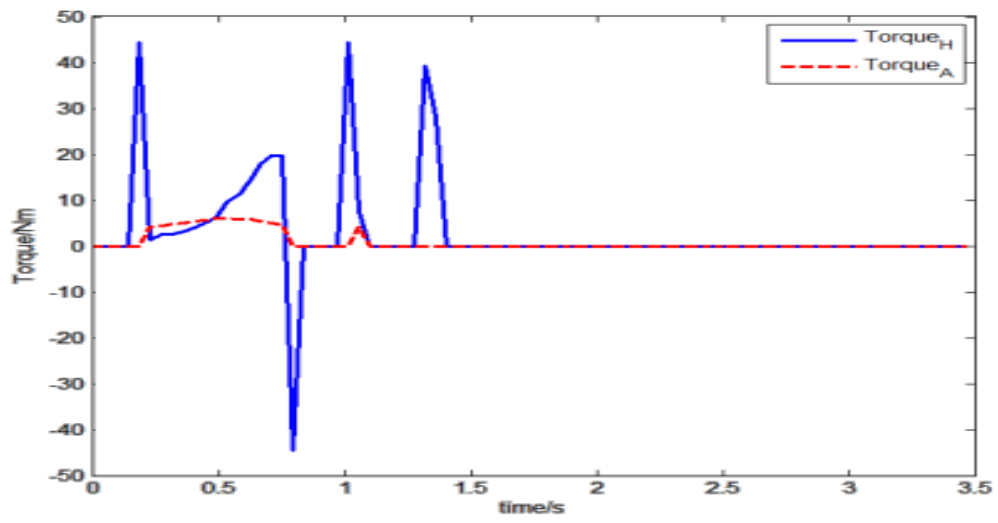


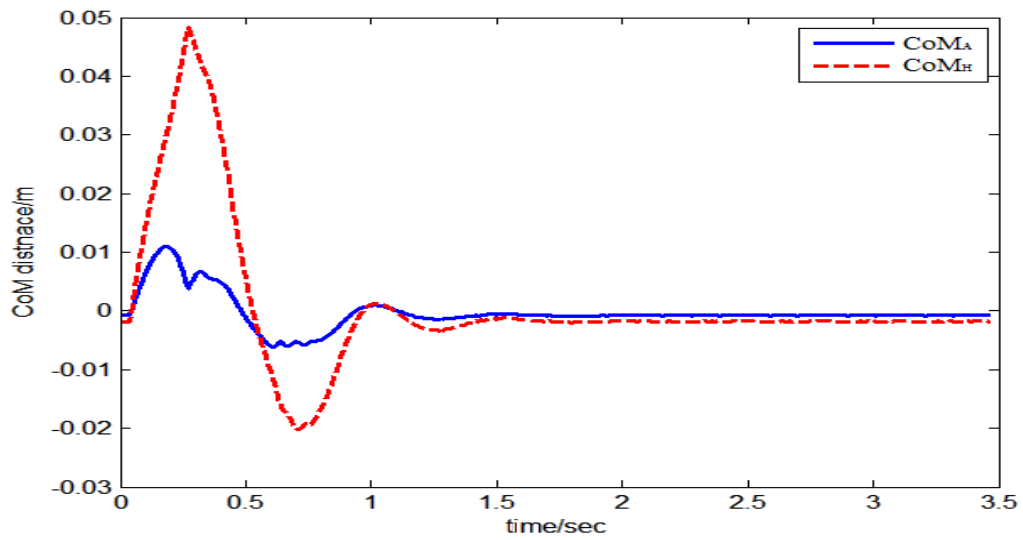
Figure 29. Simulation results for a forward push



a) Angular Deflection



b) Applied Torque



c) CoM_A and CoM_H Deflection

Figure 30. Response of the humanoid robot to the applied push

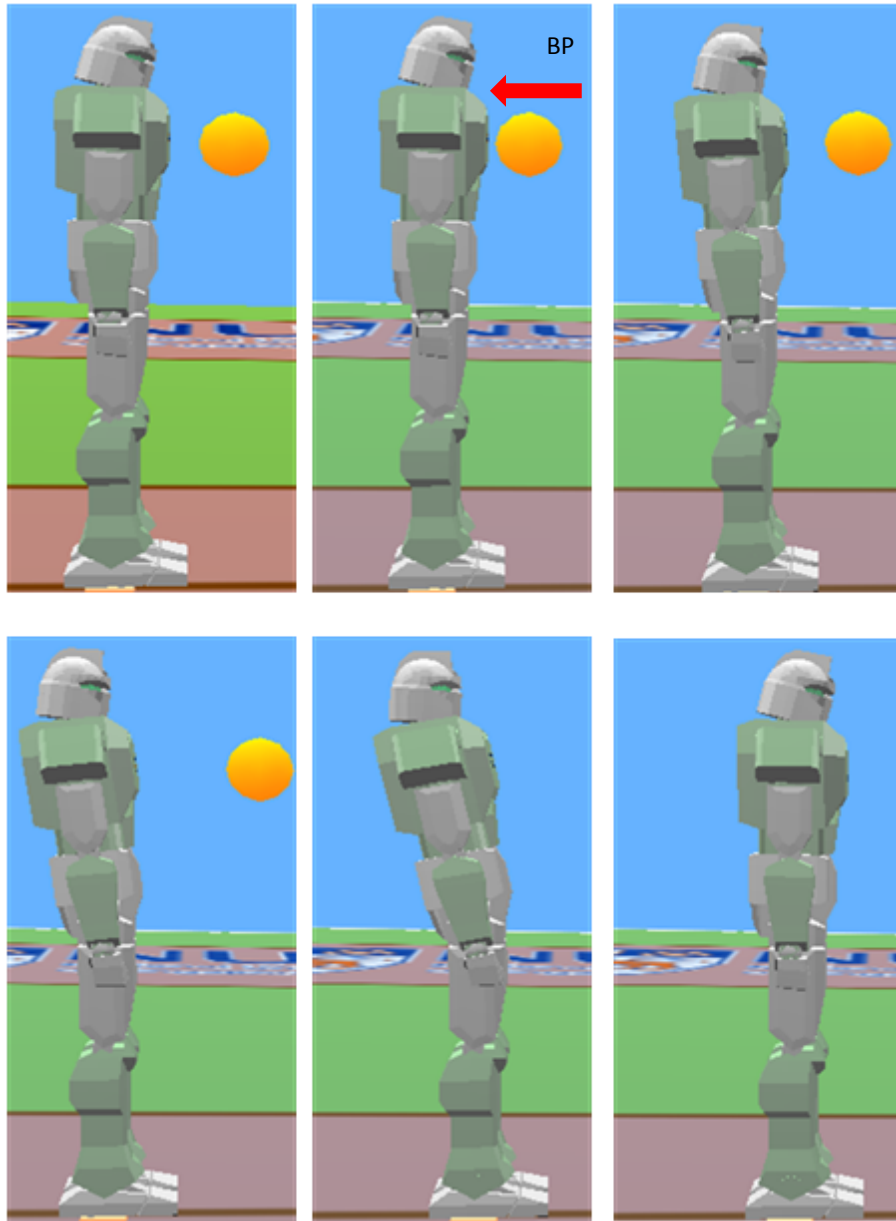
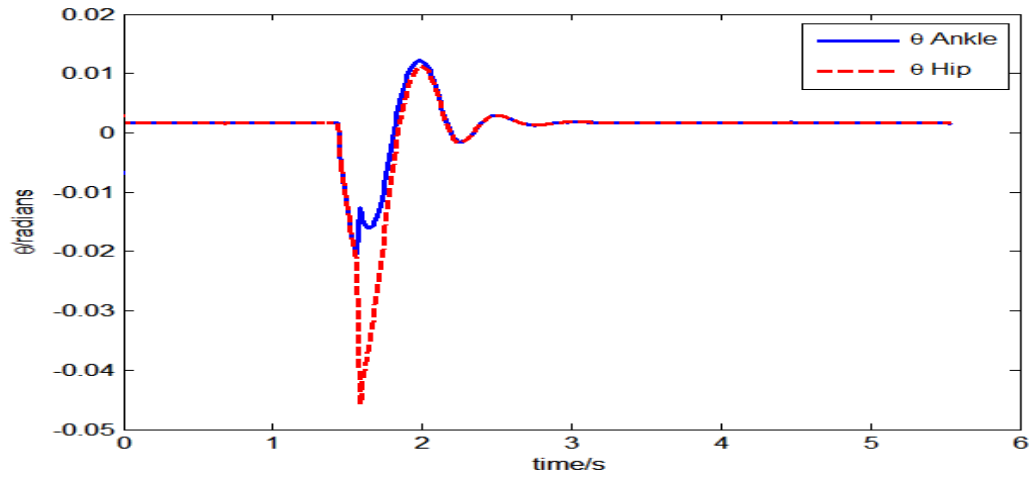
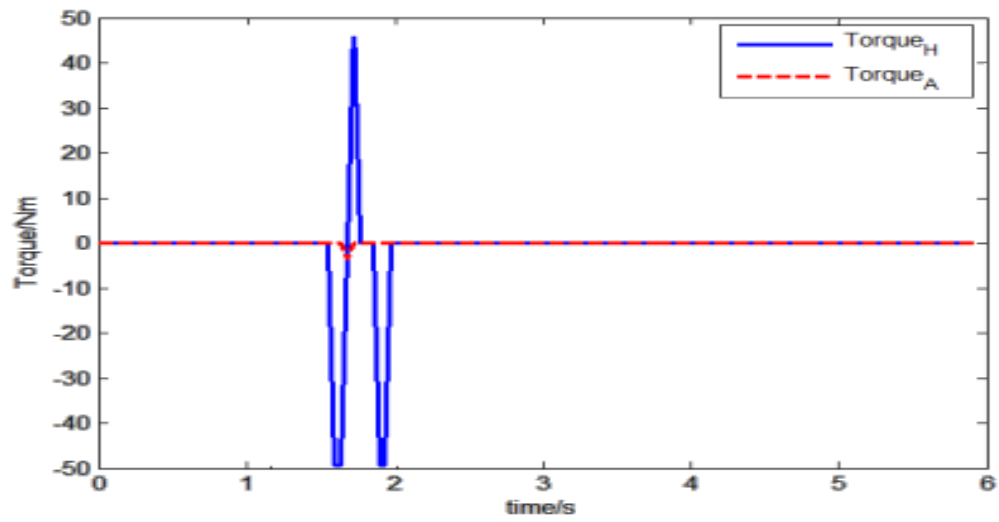


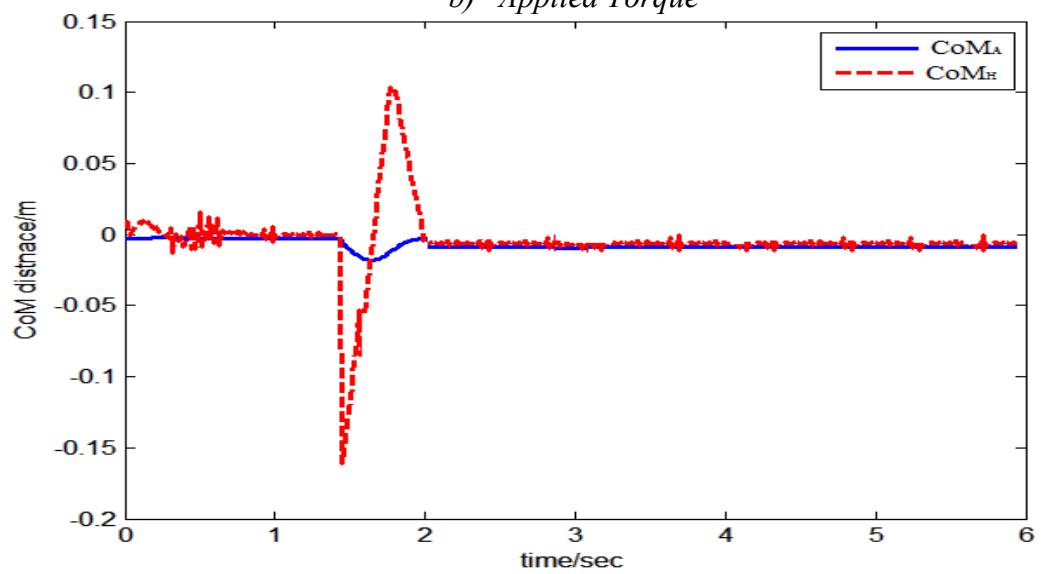
Figure 31. Response of the humanoid robot to the applied backward push



a) Angular Deflection



b) Applied Torque



c) CoM_A and CoM_H Deflection

Figure 32. Response of the humanoid robot to the applied push

The phase plot shows the stability margin for CoM_{AVG} of the simulated robot for multiple trajectories with varying magnitude of force applied. The stable and unstable regions have been achieved by experimentation on the simulator, for multiple trajectories with varying magnitudes of force applied. The shaded area in this figure corresponds to the unstable region. The trajectory plot in the figure below shows that disturbances causing an instantaneous CoM_{AVG} velocity shift beyond 0.45ms^{-1} , leads to an unstable trajectory. Such levels of disturbance should be catered by taking a step, which is beyond the scope of this work.

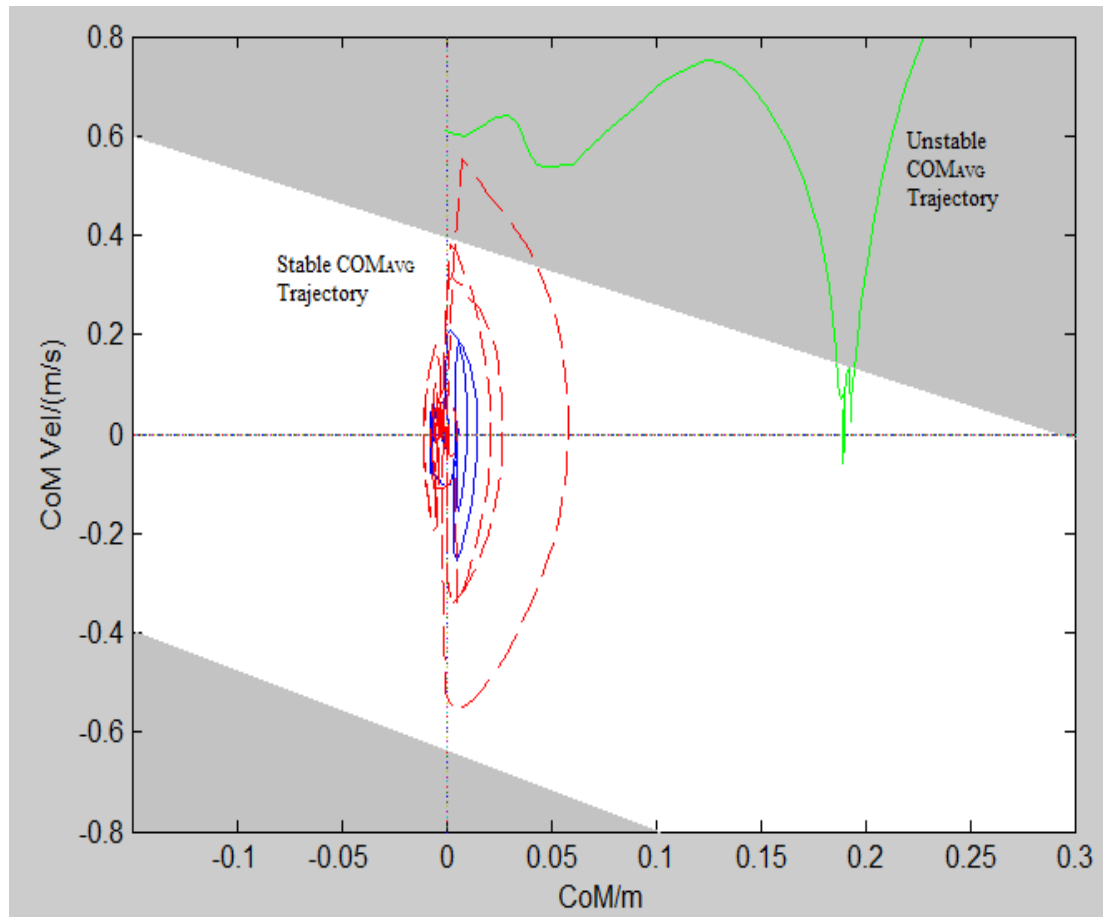
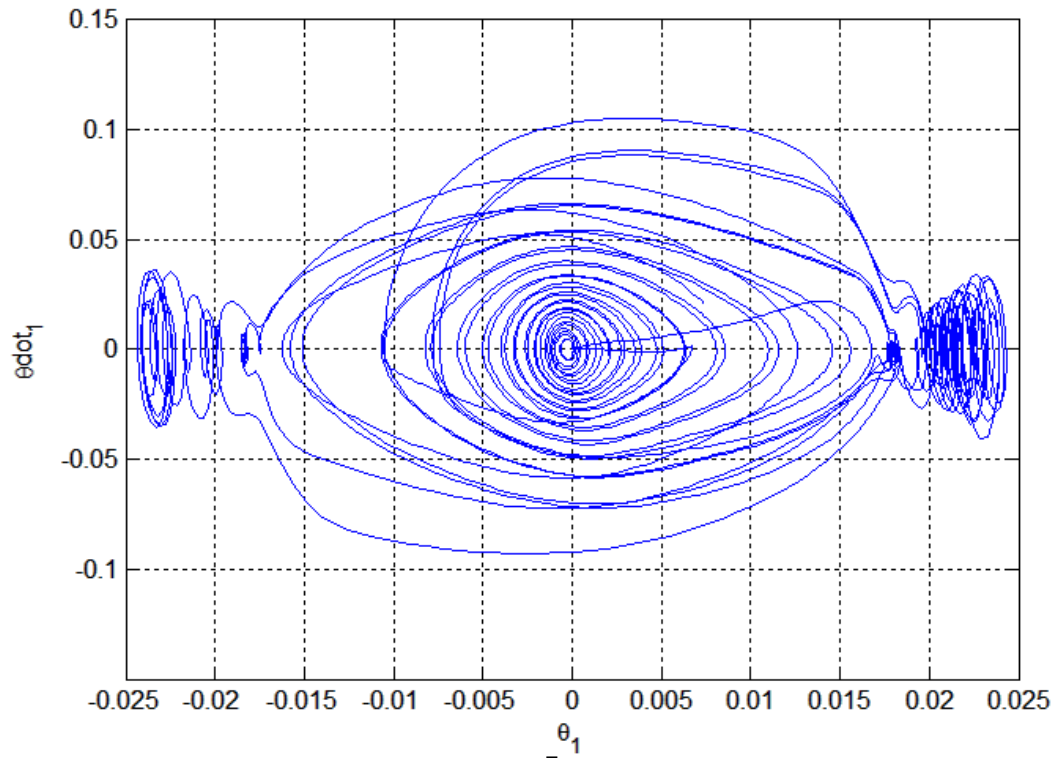
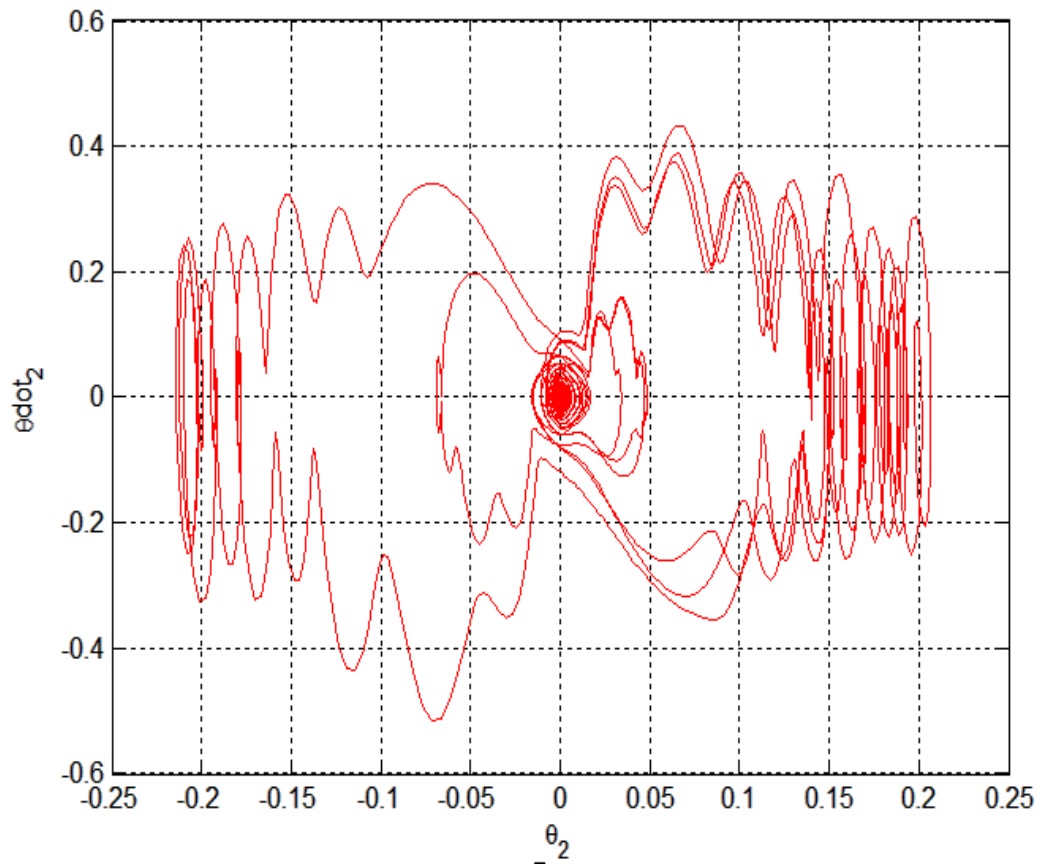


Figure 33. Phase plot for multiple trajectories of CoM_{AVG}



a) Phase Plot for $(\Theta_I - 1.57)$ and $\dot{\Theta}_I$



b) Phase Plot for Θ_2 and $\dot{\Theta}_2$

Figure 34. Phase plots for state x for multiple trajectories

The phase plots shown in Figures 34 reflect the stabilization of the controlled states of the system, which converge at respective equilibrium states for multiple trajectories. These graphs also depict the common range of variation induced by the disturbance, that the controller is capable of handling.

7.4 Experimental Evaluation on NUSBIP-III ASLAN

7.4.1 Hardware Platform

The robot NUSBIP-III ASLAN at NUS is used for implementation of the controller designed above. ASLAN is a human sized humanoid robot equipped with DC servo motors which are controlled through ELMO amplifier. PC/104 is the major processing unit with a processing frequency of 100Hz, which communicates with ELMO through CAN BUS. The robot is equipped with accelerometer and gyroscope to provide inertial measurement. Rotational measurements are sensed through encoders mounted at the motors.

7.4.2 Implementation Details

The servos of the robot are operated in current mode, where the commanded current is determined as follows,

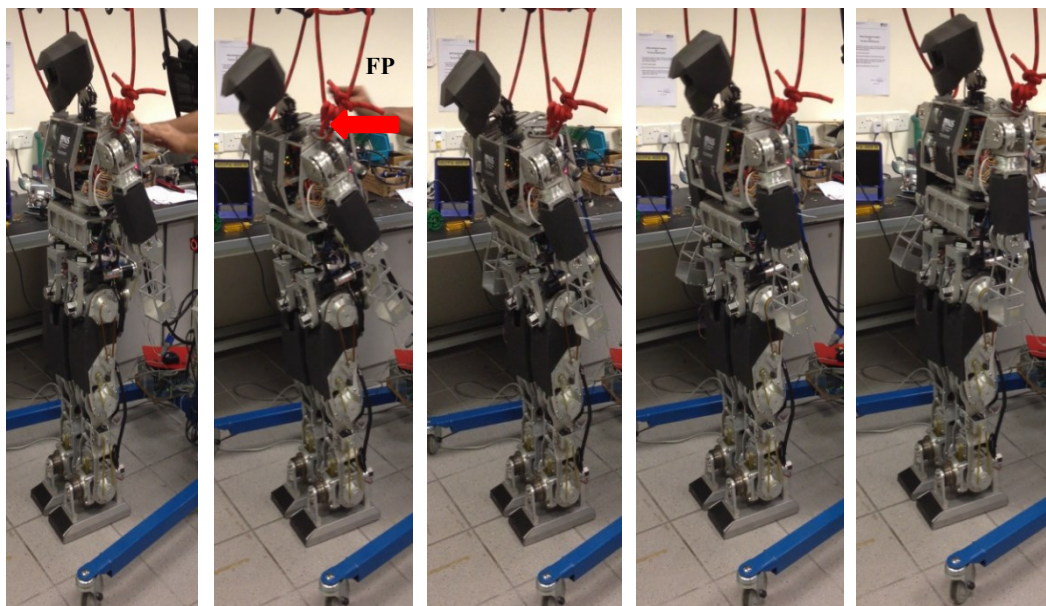
$$i = \frac{\tau}{K_T N}$$

where K_T and N represent torque constant specified in the motor datasheet, and gear ratio respectively.

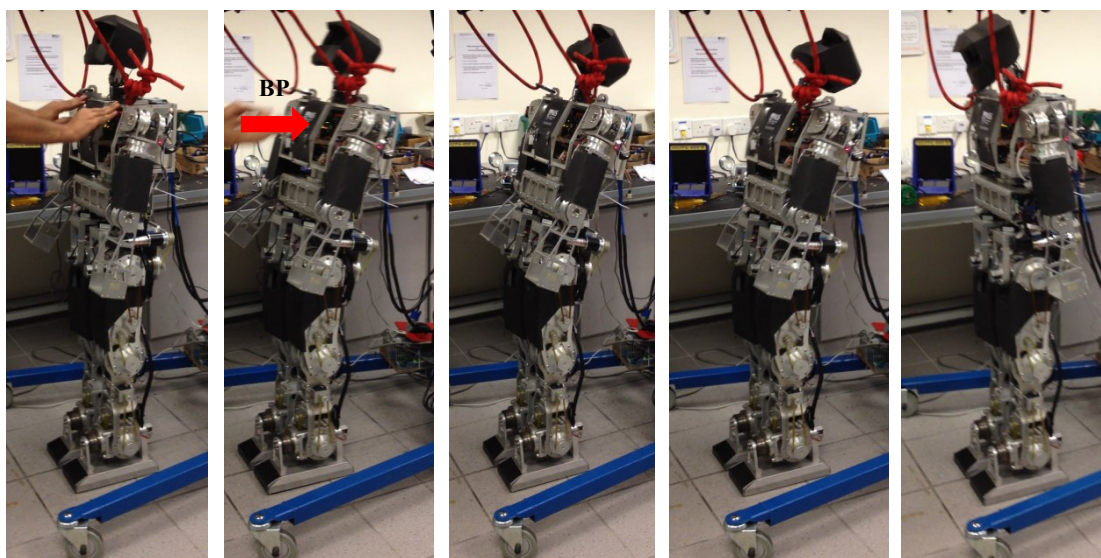
Since the total weight and size of the simulated and actual robots are different, gains for linear and non-linear controllers are recomputed. The gains used for the NCPFL are $K_{vD} = 45$, and $K_{vP} = 5$. The LQR values for Q and R matrices for state space model are given as $Q = I(4 \times 4)$ and $R = 10e^{-12}$. The L matrix is defined as $L = [10.15, 165.8, -15.29, -7.250]$. The gains employed at the ankle for PD control are defined as $K_{DA} = 0.5$, and $K_{PA} = 55$.

7.4.3 Result Evaluation

Figure 35 shows response to a push applied from front and back, while Figures 36 and 37 show how the angles, current and CoM of each link of the humanoid robot vary with respect to time. Graphs in Figure 38 shows response of the robot for multiple push imparted to the humanoid from front and back. It can be seen from Figure 38b that the maximum ankle current employed is $-1.5 < i_A < 1.5$ amperes where the ankle motor has the capacity to provide up to 6 amperes of continuous current. Thus it is hypothesized that the current employed through PD controller assists to overcome ankle friction components during upper body movements determined by NCPFL.

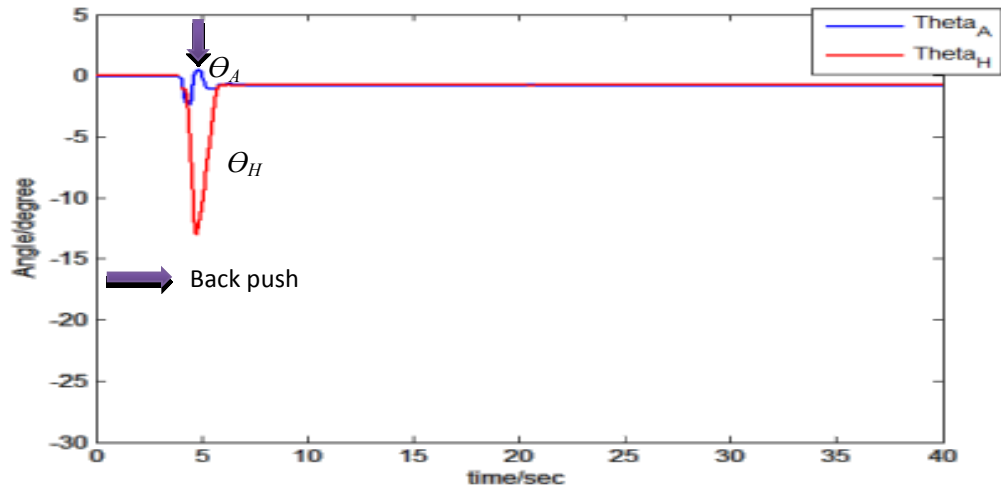


a) *Front Push*

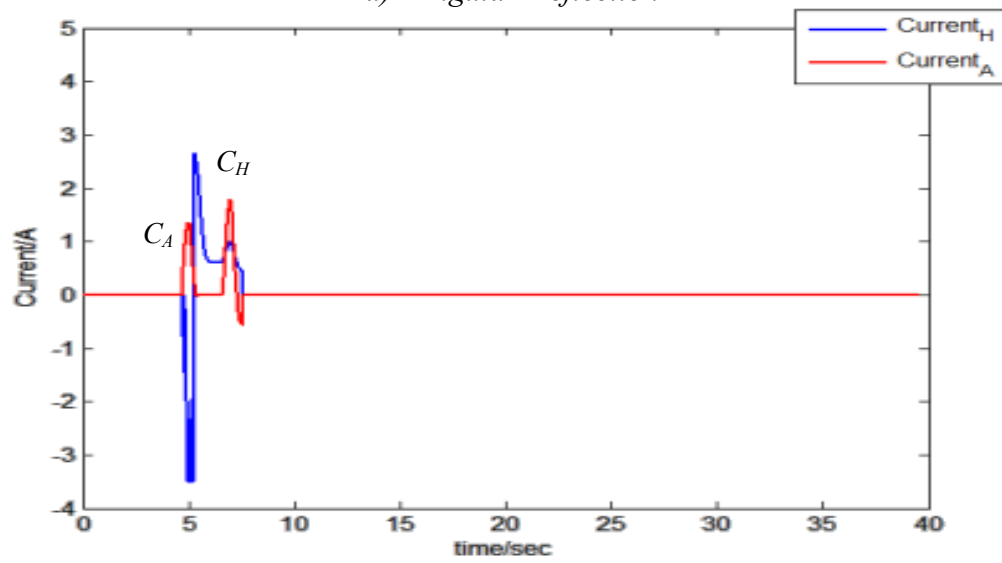


b) *Back Push*

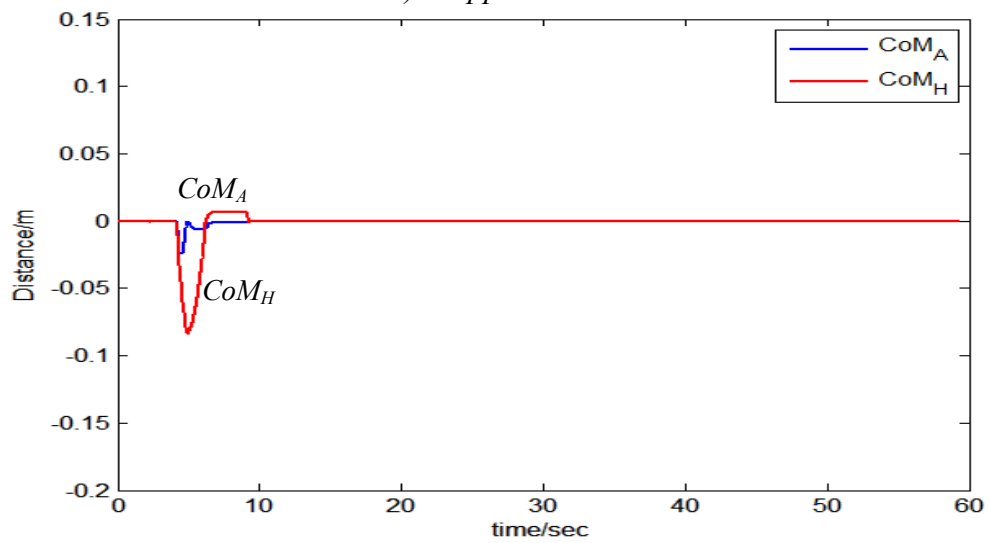
Figure 35. Response of humanoid robot ASLAN to a push from front and back



a) Angular Deflection

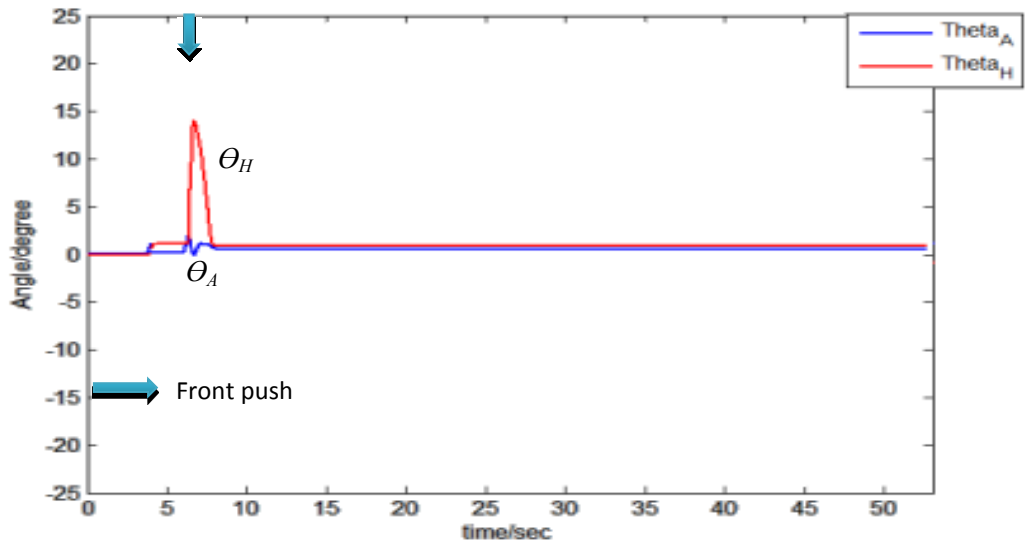


b) Applied Current

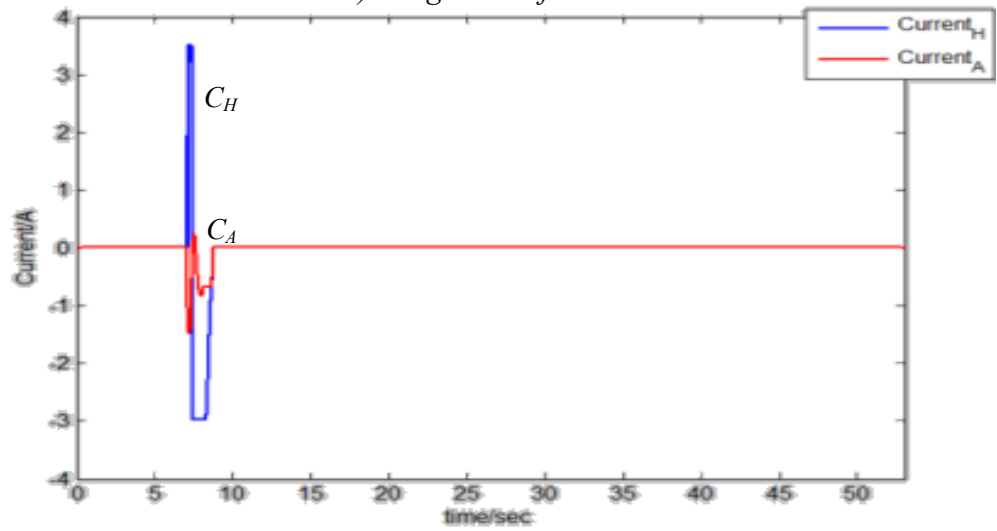


c) CoM_A and CoM_H Deflection

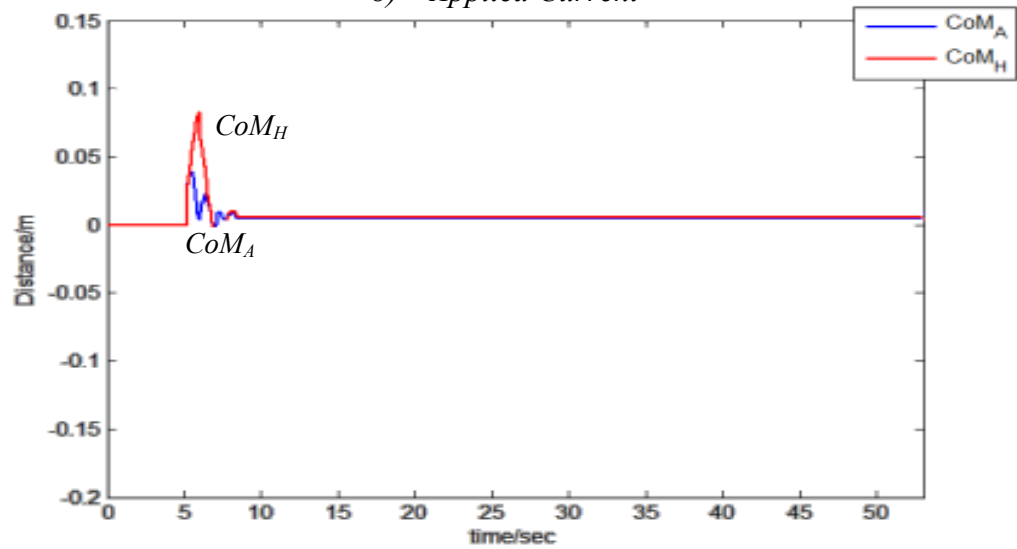
Figure 36. response of humanoid robot ASLAN to a forward push



a) Angular Deflection

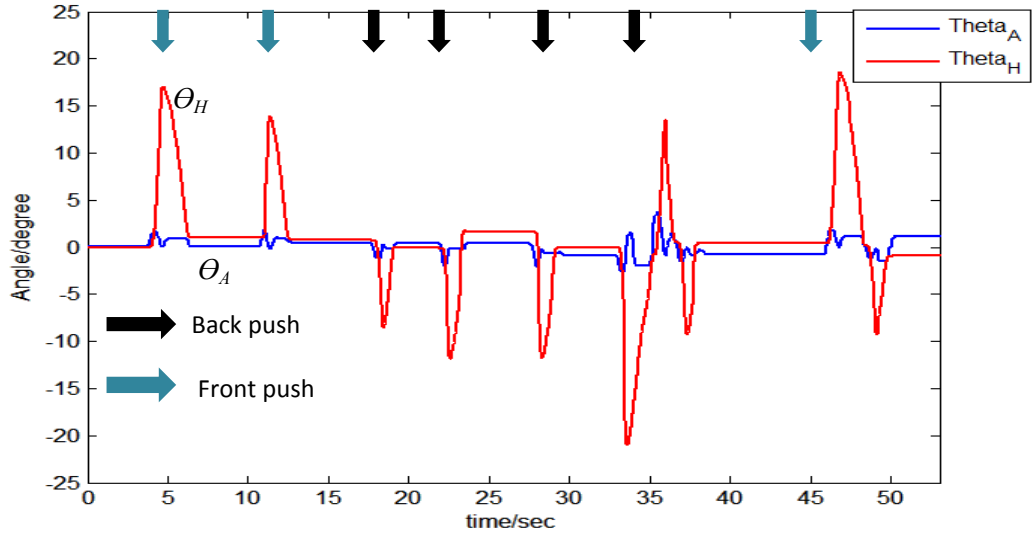


b) Applied Current

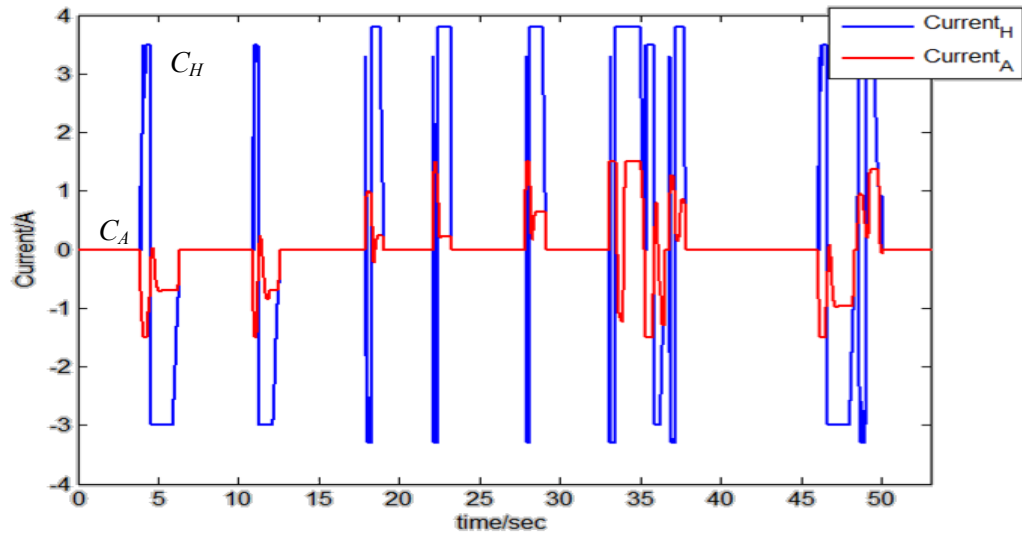


c) CoM_A and CoM_H Deflection

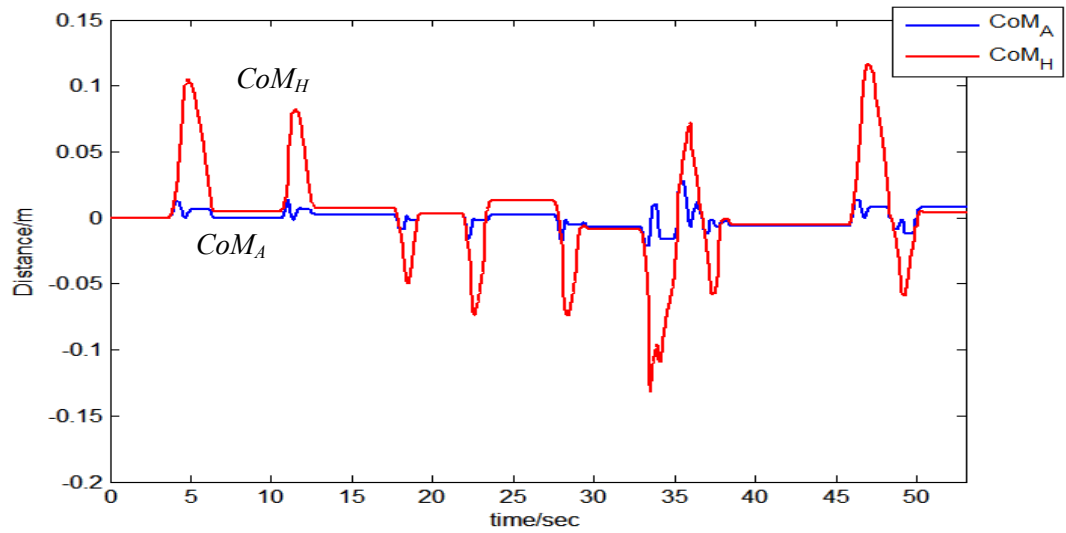
Figure 37. Response of humanoid robot ASLAN to a backward push



a) Angular Deflection



b) Applied Current



c) CoM_A and CoM_H Deflection

Figure 38. Response of the robot to multiple consecutive trajectories

7.5 Performance Comparison with Passive Ankles

The proposed control architecture has been designed for an acrobot model which implies passive ankles for the robot. In the previous section, a PD controller was proposed to cater friction components at the ankle joint. This section completely removes any torque provided to the ankle and evaluates performance of various controllers under such “zero ankle torque” conditions. There are two objectives behind this experimentation. First, a comparison is conducted between NCPFL and other algorithms to compare the efficiency of the proposed algorithm. Second, it is proved that the torque provided to the ankle in the complete control strategy is indeed used only for friction compensation.

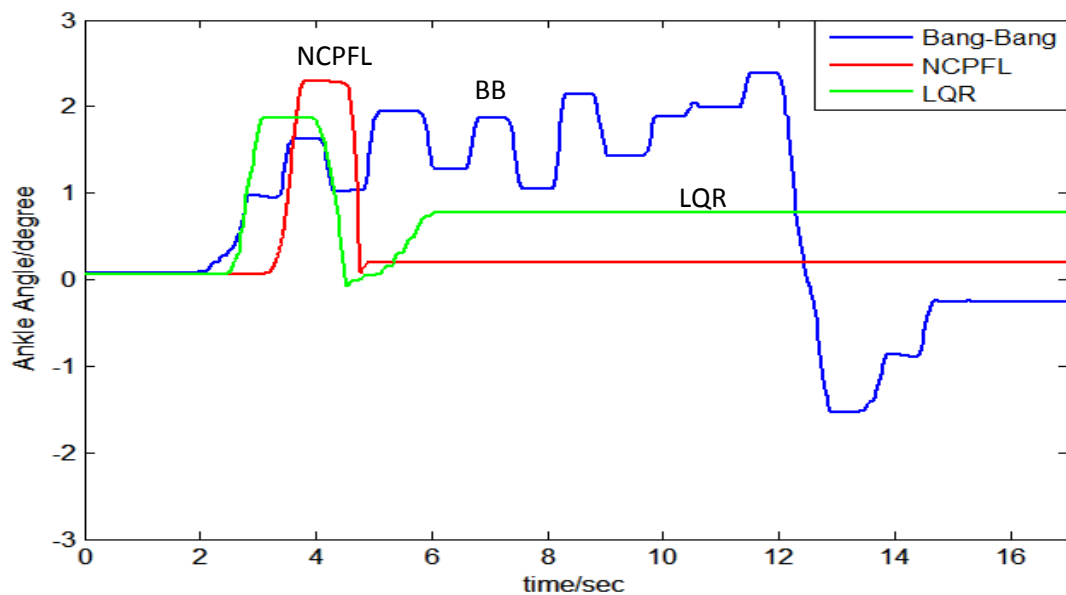


Figure 39. Performance Comparison with Passive Ankle Joint

NCPFL is implemented on the humanoid robot, compared with LQR and *Bang-Bang* [30] control approach. *Bang-Bang* controller is chosen since it is a common controller

opted for the implementation of the '*hip strategy*'. The results obtained from this experimentation have been shown in Figure 39 and 40. The graphs show that *Bang-Bang* (BB) leads to oscillation before stabilization. This is because BB defines a fixed maximum and minimum current value for ankle restoration. LQR is able to restore the ankle, to a certain extent, but the convergence range over CoM_A is very limited. For higher ankle deflection, it commands current which is out of bounds for the actuators. Thus NCPFL proves to be a better option for the control of passive ankle through the hip joint.

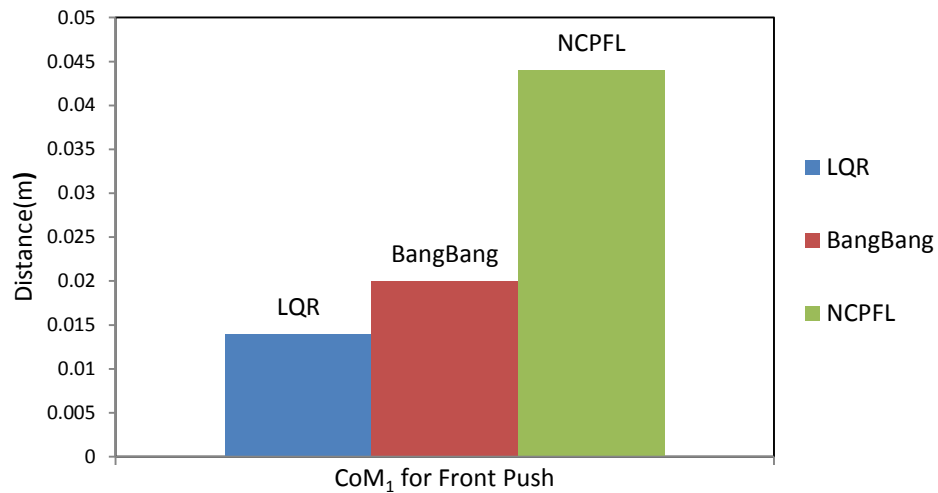


Figure 40. Performance Range for Controllers under Passive Ankle Joint

Despite having the ability of restoration, it is observed during experimentation that a standalone NCPFL strategy with zero ankle torque employs large rotation of the upper body. Whereas, a small amount of regulating current at the ankles can significantly decrease this upper body bend. The hypothesized reason is associated with compensation of friction at the non-back drivable ankle joint which requires a larger jolt from the upper body under high friction. Thus the complete architecture for

push recovery includes an ankle torque controller, to facilitate control attempted through the hip joint.

7.6 Conclusion

In this chapter, a synergy of NCPFL and LQR control is presented as an efficient means to regulate posture of the humanoid robot, when pushed. The proposed strategy has been tested in Webots and experimentally verified on NUSBIP-III ASLAN. A comparative analysis of the controller is provided, with other common control strategies. This analysis provides beneficial insights into practical considerations that need to be accounted for, in a position controlled humanoid, with essentially stiff joints, when implementing stabilizing control.

Possible future work can include extension of this algorithm to take into consideration the knee joint as part of the stabilization process, since knee plays an important role in human stabilization techniques. The two link model can be extended to three links and may be compared with the work presented in this paper.

BIBLIOGRAPHY

- [1] Boston dynamics, Petman, [online] <http://www.terminatorrobots.com/p=61>, 2012.
- [2] Team DRC-HUBO for DARPA Robotics challenge, [online] [http:// spectrum .ieee.org/autoton/robotics/humanoids/team-drc-hubo-darpa-robotics-challenge](http://spectrum.ieee.org/autoton/robotics/humanoids/team-drc-hubo-darpa-robotics-challenge), 2013.
- [3] Honda, ASIMO, [online] [http://commons.wikimedia.org/wiki/File: 2005_Honda _ASIMO_02 .JPG](http://commons.wikimedia.org/wiki/File:2005_Honda_ASIMO_02.JPG), 2012.
- [4] R. Tedrake, “Underactuated robotics: Learning, planning and control for efficient and agile machines”, Course notes for MIT 6.832, *Masachusetts Institute of Technology*, 2009.
- [5] Tiptoe maneuver, [online] <http://midoyoga.com/content/foot>, 2012.
- [6] Miomir Vukobratovic and Branislav Borovac. “Zero-moment point – thirty five years of its life”. *International Journal of Humanoid Robotics*, 1(1):157-173, 2004.
- [7] University of Michigan, Mabel, [online] <http://www.gizmag.com/mabel-the-running-robot/19558/> , 2012.
- [8] National Institute of Advanced Science and Technology, HRP, [online] <http://www.howtowe.com/blog/918101> , 2012.
- [9] A. Goswami. “Postural stability of biped robots and the foot rotation indicator (FRI) point”. *International Journal of Robotics Research*, 18(6), 1999.
- [10] S. H. Collins, A. Ruina, R. Tedrake, and M. Wisse. “Efficient bipedal robots based on passive-dynamic walkers”. *Science*, 307:1082-1085, February 18 2005.
- [11] A. Goswami, B. Espiau, and A. Keramane. “Limit cycles and their stability in a passive bipedal gait”. Pages 246-251. *IEEE International Conference on Robotics and Automation (ICRA)*, 1996.

- [12] J. Morimoto, J. Nakanishi, G. Endo, G. Cheng, C. G. Atkeson, G. Zeglin. "Poincare-map-based reinforcement learning for biped walking". In *Proceedings of IEEE International Conference on Robotics and Automation*, 2005.
- [13] J. Pratt, J. Carff, S. Drakunov and A. Goswami. "Capture Point: A step toward humanoid push recovery". In 6th IEEE-RAS International Conference on Humanoid Robots, December 2006, pp. 200-207.
- [14] T. Koolen, T. D. Boer, J. Rebula, A. Goswami, and J. E. Pratt. "Capturability-based analysis and control of legged locomotion. Part 1: Theory and application to three simple gait models". *International Journal of Robotics Research*, 2012.
- [15] J. E. Pratt, T. Koolen, T. D. Boer, J. Rebula, S. Cotton, J. Carff, M. Johnson, and P. Neuhaus. "Capturability-based analysis and control of legged locomotion, part 2: Application to m2v2, a lower-body humanoid". *International Journal of Robotics Research*, 2012.
- [16] J. Pratt and R. Tedrake. "Velocity based stability margins for fast bipedal walking". In First Ruperto Carola Symposium in the *International Science Forum* of the University of Heidelberg entitled "*Fast Motions in Biomechanics and Robots*", Heidelberg Germany, September 7-9 2005.
- [17] Bioloid GP [online]<http://www.robotshop.com/bioloid-gp-grand-prix-humanoid-robot-3.html>, 2012.
- [18] Darwin Robot [online]<http://www.ubergizmo.com/2010/12/darwin-op-might-change-the-world-of-robotics/>, 2012.
- [19] C. Ott, M.A. Roa and G. Hirzinger, "Posture and balance control for biped robots based on contact force optimization," *Proc. IEEE-RAS Int. Conference on Humanoid Robots*, pp.26-33, 2011.

- [20] S. Hyon and G. Cheng. “Passivity-based Full-body Force Control for Humanoids and Application to Dynamic Balancing and Locomotion”. In *Proc. Of IEEE/RSJ International Conference on Intelligent Robots and Systems*, Beijing, China, Oct. 2006, pp. 4915-4922.
- [21] S. H. Hyon, J. G. Hale and G. Cheng, “Full-body compliant human humanoid interaction: Balancing in the presence of unknown external forces,” *IEEE Transactions on Robotics*, vol 23, pp. 884-898, October 2007.
- [22] A. Albu-Schaffer, C. Ott, and G. Hirzinger, “A unified passivity-based control framework for position, torque and impedance control of flexible joint robots,” *International Journal of Robotics Research*, vol. 26, no. 1, pp. 23-29, January 2007.
- [23] C. Ott, A. Albu-Schaffer, A. Kugi, and G. Hirzinger. “On the passivity based impedance control of flexible joint robots”. *IEEE Transactions Robotics*, vol. 24, no. 2, pp. 416-429, 2008.
- [24] B. J. Stephens and C. G. Atkeson, “Dynamic balance force control for compliant humanoid robots,” in *Proc. of International Conference on Intelligent Robots and Systems*, 2010.
- [25] S. -h. Lee and A. Goswami, “Ground reaction force control at each foot: A momentum-based humanoid balance controller for non-level and non-stationary ground,” in *IEEE/RSJ International Conference on Intelligent Robots and Automation*, May 2009, pp. 4423-4429.
- [26] C. Atkeson and B. Stephens, “Multiple balance strategies from one optimization criterion,” in *The IEEE-RAS 2007 International Conference on Humanoid Robots*, 2007.

- [27] J. Wang, "Humanoid push recovery with robust convex synthesis," in *IEEE/RSJ International Conference on Intelligent Robots and Systems*, Oct. 2012.
- [28] Linear inverted pendulum, Double linear inverted pendulum models, [online] <http://www.sciencedirect.com/science/article/pii/S0021929012005064>.
- [29] S. Kajita and K. Tani. "Study of dynamic biped locomotion on rugged terrain-derivation and application of the linear inverted pendulum mode". *Proceedings of IEEE International Conference on Robotics and Automation*, vol. 2, pp. 1405-1411, 1991.
- [30] H. Hemami and P. Camana. "Nonlinear feedback in simple locomotion systems". *IEEE Transactions on Biomedical Engineering*, pp. 25-36, 1970.
- [31] B. Stepehns, "Humanoid push recovery", *IEEE-RAS International Conference on Humanoid Robotics*, Pittsburgh, 2007.
- [32] T. de Boer, "*Foot placement in robotic bipedal locomotion*". Phd Thesis, Delft University of Technology, 2012.
- [33] D. Winter, "Human balance and posture control during standing and walking," *Gait and Posture*, vol. 3, no. 4, pp. 193-214, December 1995.
- [34] W. Huan, C. M. Chew, G. S. Hong. "Coordination in CPG and its application on bipedal walking". *IEEE International Conference on Robotics, Automation and Mechatronics*, RAM 2008, pp. 450-455.
- [35] W. Huang, C. M. Chew, G. S. Hong, N. Gnanassegarane. "Trajectory generator for rhythmic motion control of robot using neural oscillators". *Advances in Climbing and Walking Robots*, pp. 383-392.
- [36] W. Huang, C. M. Chew, Y. Zheng, G. S. Hong. "Pattern generation for bipedal walking on slopes and stairs". *IEEE-RAS International Conference on Humanoid Robots (Humanoids)*, pp. 205-210, 2008.

- [37] H. W. Wei, “Exploiting the inherent coordination of central pattern generator in the control of humanoid robot walking”. Phd Thesis, National University of Singapore, 2010.
- [38] M.W. Spong. “Partial feedback linearization of underactuated mechanical systems”. *Proceedings of IEEE International Conference on Intelligent Robots and Systems*, pp. 314-321, 1994.
- [39] M. Grotjahn, M. Daemi, and B. Heimann. “Friction and rigid body identification of robot dynamics”. *International Journal of Solids Structure*, vol. 38, pp. 10-13, 2001.
- [40] H.-W. Park, K. Sreenath, J. W. Hurst and J. W. Grizzle. “Identification and dynamic model of a bipedal robot with a cable-differential-based compliant drivetrain”. Technical Report CGR 10-06, University of Michigan Control Group, 2010.
- [41] N. Lakbakbi El Yaaqoubi, and G. Abba. “Identification of physical parameters including ground the model parameters of walking robot rabbit”. *Proceedings of 9th IEEE-RAS International Conference on Humanoid Robots* Paris, France, pp. 269 -276, 2009.
- [42] F. Reyes and R. Kelly. "On parameter identification of robot manipulator". *IEEE International Conference on Robotics and Automation*, Albuquerque, New Mexico, April. pp. 1910-1915, 1997.
- [43] G. Venture, K. Ayusawa, and Y. Nakamura. “A numerical method for choosing motions with optimal excitation properties for identification of biped dynamics—an application to human”. in *IEEE International Conference on Robotics and Automation*, pp. 1226–1231, 2009.

- [44] K.-J. Park. "Fourier-based optimal excitation trajectories for the identification of robots". *Robotica*, vol.24, pp. 625-633, 2006.
- [45] J. Swevers, C. Ganseman, B. D. Tükel, J. De Schutter, and H. Van Brussel, "Optimal robot excitation and identification", *IEEE Transaction on Robotics and Automation*, vol. 13, pp.730 -740, 1997.
- [46] M. Gautier and W. Khalil. "Exciting trajectories for the identification of base inertial parameters of robots". *International Journal of Robotics Research*, vol. 4, no. 11, pp. 363–375, 1992.
- [47] J. Swevers, W. Verdonck, and J. D. Schutter, "Dynamic model identification for industrial robots: Integrated experiment design and parameter estimation," *IEEE Control Systems Magazine*, vol. 27, no. 5, pp. 58–71, 2007.
- [48] C. H. An, C. G. Atkeson, and J. M. Hollerbach. "Estimation of inertial parameters of rigid body links of manipulators", *24th Conference on Decision and Control*, 1985.
- [49] K. Ayusawa, G. Venture, and Y. Nakamura. "Identification of humanoid robots dynamics using floating base motion dynamics". in *IEEE/RSJ International Conference on Intelligent Robots and Systems*, pp. 2854–2859, 2008.
- [50] M. Mistry, S. Schaal, and K. Yamane, "Inertial parameter estimation of floating base humanoid systems using partial force sensing," in *IEEE-RAS International Conference on Humanoid Robots*, pp. 492–497, 2009.
- [51] J.-J. Slotine and W. Li. "On the adaptive control of robot manipulators". *International Journal of Robotics Research*, pp. 49-59, 1987.
- [52] R. Ortega, M. W. Spong, "Adaptive Motion Control of Rigid Robots: a Tutorial", 1989.

[53] Webots, <http://www.cyberbotics.com>, commercial Mobile Robot Simulation Software. [Online]. Available:<http://www.cyberbotics.com>.